NASA TECHNICAL MEMORANDUM

NASA TM 75276

EXPERIMENTAL STUDIES ON THE INFLUENCE OF THE DEGREE OF TURBULENCE AND OF A TURBULENCE THREAD ON THE COMPRESSIBLE SUBSONIC FLOW THROUGH FLAT COMPRESSOR CASCADES

K. Barsun

Translation of "Experimentelle Untersuchungen über den Einfluss der turbulenzgrades und eines Turbulenzfadens auf die kompressible Unterschallstromung durch ebene Verdichtergitter," Report 68/34, Institut fuer Aerodynamik Deutsche Forschungsanstalt fur Luft-und Raumfahrt (DFL), Braunschweig, 1968, pp. 1-68.

NATIONAL AERONAUTICS AND SPACE ADMINISTRATION
WASHINGTON, D.C. 20546 JULY 1978

STANDARD TITLE PAGE

1. Report No. NASA TM 75276	2. Government Accession No.	3. Recipient's Catalog No.
4. Title and Subtitle EXPERIMENTAL STUDIES ON THE INFLUENCE OF THE DEGREE OF TURBULENCE AND OF A TURBULENCE THREAD ON THE COMPRESSIBLE SUBSONIC FLOW THROUGH FLAT COMPRESSOR CASCADES		5. Report Date July, 1978 6. Performing Organization Code
7. Author(s) K. Barsun, Institute for Aerodynamics, German Aeronautics and Space Research Center		8. Performing Organization Report No. 10. Work Unit No.
9. Performing Organization Name and Address Leo Kanner Associates Redwood City, California, 94063		11. Contract or Grant No. NASw-2790 13. Type of Report and Period Covered Translation
12. Sponsoring Agency Name and Address National Aeronautics and Space Administration, Washington, D.C. 20546		14. Sponsoring Agency Code

15. Supplementary Notes

Translation of "Experimentelle Untersuchungen über den Einfluss der turbulenzgrades und eines Turbulenzfadens auf die kompressible Unterschallstromung durch ebene Verdichtergitter," Report 68/34, Institut fuer Aerodynamik, Deutsche Forschungsanstalt für Luft-und Raumfahrt (DFL), Braunschweig, 1968, pp. 1-68, [DFL Report 0509]

16. Abstract

The measurements revealed that at low Reynolds numbers the profile loss is considerably reduced both by the increased degree of turbulence and by a turbulence thread, while it is somewhat increased at high Reynolds numbers, and that a profile loss reduction is connected with an increase in deflection and in pressure shift.
The turbulence generator is most effective on the one hand in the middle of the operating range of the cascades, and on the other at very high Mach numbers together with a large angle of incidence.

17. Key Words (Selected by Author(s))	18. Distribution Statement
	Unclassified-Unlimited

19. Security Classif. (of this report)	20. Security Classif. (of this page)	21. No. of Pages	22. Price
Unclassified	Unclassified	69	

Table of Contents

EXPERIMENTAL STUDIES ON THE INFLUENCE OF THE DEGREE OF TURBULENCE AND OF A TURBULENCE THREAD ON THE COMPRESSIBLE SUBSONIC FLOW THROUGH FLAT COMPRESSOR CASCADES

K. Barsun
Institute for Aerodynamics, German Aeronautics and Space Research Center, Braunschweig

Synopsis

The study concerns the influence of an increased degree of in the oncoming flow and the influence of a turbulence thread placed on the vane suction side on the flow through two straight compressor cascades. The cascades consist of profiles NACA 65-608 and NACA 65-612 with a vane angle of $\beta_s = 130°$ (measured against the cascade front) and a spacing ratio of $t/l = 1$.

The study included wake and pressure distribution measurements and were carried out at Reynolds numbers of $Re_1 = 1 \times 10^5$ and 4×10^5, angles of incidence between $\beta_1 = 130°$ and 148° and at mach numbers between $Ma_1 = 0.3$ and 0.9.

The measurements revealed that at low Reynolds numbers the profile loss is considerably reduced both by the increased degree of turbulence and by a turbulence thread, while it is somewhat increased at high Reynolds numbers, and that a profile loss reduction is connected with an increase in deflection and in pressure shift.

The turbulence generator is most effective on the one hand in the middle of the operating range of the cascades, and on the other at very high Mach numbers together with a large angle of incidence.

---

* Numbers in the margin indicate pagination in the foreign text.

1. Introduction

As everyone knows, turbulence boundary layers can tolerate a considerably greater increase in pressure without separation than laminaryboundary layers. Therefore, it is of critical importance for flows through retarding vane cascades whether the boundary layers on the bladesaare laminar or turbulent and how the laminary-turbulent transition proceeds.

Since the calculation of the transition has so far not been solved for all cases, one still has to fall back on measurements in studying this problem for blade cascades. For this reason, the high velocity cascade wind tunnel of the German Aeronautics and Space Research Center is well suited for this because it allows the Mach number and Reynolds number of the cascade flow to be varied independently of one another. On the other hand, however, measurement facilities for direct boundary layer measurements on the blade cascades are not available so that these studies remain restricted to wake and pressure distribution measurements.

Using this wind tunnel, studies have been done in past years on the influence of the degree of turbulence and of the surface roughness on the flow through straight vane cascades.

The studies on turbine cascades (NACA 8410) are summarized in [1]. As a followup to this, two compressor cascades made of profile NACA 65-608 and NACA 65-612 were studied with different types of turbulence [2], to be sure only at one angle of incidence in the middle of the operating range.

This report concerns the extension of the studies described in [2], to the entire useful angle of incidence range of both compressor cascades. The measurements were carried out in the high velocity cascade wind tunnel between March and July, 1966.

In addition, a few measurements with incompressible flow, which were carried out as preliminary studies to [2], are evaluated in this report and compared with the results obtained by J. Bahr [3,4]. /4

The experiment covered in report [2] and in this report, insofar as they concern compressible flow, were reported on in a brief paper (formal contribution) at the Royal Society Conference on Internal Aerodynamics (Turbo-machinery) "Wates Foundation" in Cambridge, England, July 19-21, 1967.

2. Notation (See Fig. 1)

This list contains the most important variables; additional symbols are explained in the text.

2.1 Geometric Variables

l	chord length
t	cascade spacing
t/l	cascade spacing ratio
d	greatest profile thickness
d/l	profile thickness ratio
h	vane height (span width)
h/l	vane aspect ratio
β_S	vane angle, measured against the cascade front
$\beta_1;\beta_2$	angle of flow, measured against the cascade front deflection of flow through the cascade
$x;y$	perpendicular profile coordinates, x in the profile chord direction
$a;u;z$	rectangular cascade coordinates; a perpendicular to the cascade front, u in the direction of the cascade front, z in the span width direction
e	distance of the wake measurement plane from the vane cascade

y_f	median line ordinate /5
y_d	local profile thickness
y_S	suction side ordinate
y_D	pressure side ordinate
d_F	turbulence thread diameter
x_F	rearward position of thread (position of the turbulence thread on the profile suction side)
NACA 65-612	Profile designation, interpreted as follows: 6 serial number 5 position of the pressure minimum on the symmetric profile with parallel oncoming flow at $x/l = 0.5$ 6 camber; $c_A^* = 0.6$ 12 thickness ratio; $d/l = 0.12$.

2.2 Flow Variables

c_A^*	potential theory lift coefficient of a single median line ($t/l \triangleq \infty$) with chord parallel oncoming flow
p_o	total flow pressure
p	static flow pressure
$q = p_o - p$	dynamic flow pressure
$\hat{p}(x)$	static pressure on the blade contour
$c_{p1} = \frac{p(x) - p_1}{q_1}$	local pressure coefficient
p_{above}; p_{below}	static pressure on the bottom walls of the working section in front of the suction slots
w	flow velocity
w'	turbulent velocity fluctuation in the direction of flow
a	sound velocity of the flowing air /6
ρ	air density
ν	kinematic viscosity of the air
$Ma = w/a$	Mach number

$Re = \frac{w \cdot l}{\nu}$	Reynolds number
$Tu = \frac{1}{w} \cdot \sqrt{\overline{w'^2}} \cdot 100\ \%$	degree of turbulence in %
$\overline{w'^2}$	average value of the square variation in velocity over time
$\zeta_{V1} = \frac{p_{o1} - p_{o2}}{q_1}$	loss coefficient of the flat compressor cascades
$\frac{\Delta p}{q_1} = \frac{p_2 - p_1}{q_1}$	pressure shift of the flat compressor cascade
$\mu = \frac{\varrho_2 w_{2a}}{\varrho_1 w_{1a}}$	contraction coefficient

2.3 Indicies

1	homogeneous oncoming flow state
2	homogeneous outflow state (far behind the cascade)
2u	outflow state in the wake measurement plane
m	mean value
S	profile suction side
D	profile pressure side

3. Measurement Procedure

/7

3.1 Apparatus

The low speed cascade wind tunnel (LST) of the DFL Institute for aerodynamics is described in detail in [5], and the high speed cascade wind tunnel (HST) in [6].

The maximum air speed in the working section of the LST (if notturbulence screen is built in) is about $w_1 \approx 65$ m/s with a working section height of 250 mm and $w_1 \approx 38$ m/s with a working section height of 500 mm. The corresponding Mach numbers are

$Ma_1 \approx 0.19$ and 0.11 respectively and the corresponding Reynolds numbers $Re_1 \approx 2.5 \times 10^5$ and 1.5×10^5 respectively, with respect to a profile depth of $t = 60$ mm.

The HST stands in a chamber which can be evacuated to 0.05 ata (corresponding to an altitude of 20 km). Therefore, by changing the static pressure and dynamic pressure, the Mach number and the Reynolds number can be adjusted largely independently of one another.

Since the working sections of both tunnels have the same dimensions, the same cascade can be built into both working sections. The oncoming flow angle β_1 can be continuously adjusted, since both vane carriers of the cascade are fixed into two turntables on the end of the dise walls. The vane angle β_S is changed by turning the individual blade around its longitudinal axis.

The boundary layers on the bottom walls of both working sections can be sucked off through slots in front of the cascade. In so doing, the amount of air sucked off is set by throttle slides so that the static pressure on the bottom walls in front of the suction slots equals the static pressure on the side walls.

The boundary layers on the side walls of the working section cannot be sucked off because the existing suction facilities are not powerfullenough for this.

The total pressure p_{o1} of the oncoming flow is measured in the prechamber and the static pressure p_1 of the oncoming flow is measured through bore holes in the sidewalls of the working section. The total pressure p_{02} (u), static pressure p_2 (u) and the outflow angle β_2(u) are measured in the wake working plane /8

with a wake probe. The outflow angle is measured by setting the probe parallel to the flow direction. This setting is carried out in the range between the wake depressions and is maintained within the wake depression.

If a turbulence screen is built in between the prechamber and the working section, the total pressure of the oncoming cascade flow p_{o1} cannot be measured in the prechamber. In this case, a pitot tube is inserted into the flow through one of the turntales just in front of the cascade. The probe opening is ha halfway up the height of the working section, 50 mm from the sidewall and the same distance in front of the cascade as the p_1 boreholes. Since as a result of the built-in turbulence screen the total pressure in the z direction (span width direction) was no longer constant, the reading for p_{o1} in the wake measurements was corrected such that p_{o1} equaled the reading for $p_{o2}(\bar{y})$, which was measured behind the cascade between two wake depressions. (The wake probe is in the cross-section of the cascade, the pitot tube in front of the cascade is 100 mm away from the wake probe in the z direction.)

If no turbulence screen is built in, the degree of turbulence of the flow in the working section depends only on the size of the working section cross-section and (in the HST) on the static pressure. In the LST, the degree of turbulence for an average working section height of 350 mm is about $Tu_1 = 0.3\%$; in the HST, depending on the height of the working section and the static pressure, it lies between $Tu_1 = 0.15\%$ and 1%.

In the measurements reported in [2], a wire mesh screen was built into the parallel portion of the oncoming flow channel perpendicular to the flow and 500 mm in front of the central vane. In this arrangement, the wake depressions of the screen wires interfereddwith the measurement behind the cascade,

and for this reason in our measurements we used a turbulence screen like that shown in Fig. 2. This was built into the nozzle and produced a degree of turbulence between $Tu_1 \approx 2.5\%$ and 4.5% /9 in the working section. The degree of turbulence produced by this screen was obtained from earlier cascade experiments [7] in which the same turbulence screen was used. Fig. 3 shows the degree of turbulence for an average working section height of 350 mm. The figure shows that the degree of turbulence wtih a built-in turbulence screen also depends on the Mach number.

The degree of tubbulence in [7] was measured with DISA hot wire probes (wire diameter 0.005 mm) and with a DISA constant temperature anemometer No. 55 A 01.

3.2 The Cascades Studied

In each situation a cascade of profiles NACA 65-608 and NACA 65-612 were studied. For these profiles it was known [3,4] that with normal wind tunnel turbulence and at small Reynolds numbers small laminar separation bubbles appear on the contour. The cascade arrangement is the same as in [2], namely $t/l = 1$ and $\beta_{SS} = 130°$. The profiles and cascade arrangement are shown in Fig. 4, and the profile coordinates and location of the pressure measurement boreholes can be obtained from Tables 1 and 2.

The vanes have a profile depth of $l = 60$ mm, a height (span width) of $h = 300$ mm and an aspect ratio of $h/l = 5$. Each cascade consists of 7-8 vanes. The two central vanes each contain 12 or 13 pressure measurement boreholes on the suction side or pressure side in the cross-section, all of which lie on the same cascade flow channel.

3.3 Types of Turbulence Studied

The following types of turbulence were studied:

1) the blades have a smooth surface, oncoming flow turbulence

is normal ($Tu_1 \approx 0.15\%$ to 1%).

2) The blades have a smooth surface, oncoming flow turbulence is increased by a screen ($Tu_1 \approx 2.5\%$ to 4.5%).

3) The blades have a turbulence thread (d = 0.06 mm) on the suction side (at $x/l = 0.25$), the oncoming flow turbulence is normal ($Tu_1 \approx 0.15\%$ to 1%). /10

Case 4 (sand roughness on the profile nose), in contrast to [2], was not further investigated. On the one hand, the measurement program was not meant to be too comprehensive, and on the other it had been shown [2] that at small Reynolds numbers the sand roughness had an effect of similar size on the separation bubbles as the turbulence thread, but that at higher Reynolds numbers the additional resistance of the sand roughness is considerably greater than that of the turbulence thread.

In case 3, the pressure measurement bore hole on the suction side at $x/l = 0.25$ cannot be used because of the turbulence thread in the same place.

3.4 Measurement Program

The measurements consisteddof wake measurements over a vane spacing and pressure distribution measurements (both in cross-section),=and were carried out on the high speed cascade wind tunnel at Reynolds numbers of $Re_1 = 1 \times 10^5$ and 4×10^5. As a followup to this, using the low speed cascade wind tunnel at a Reynolds number of $Re_1 = 1 \times 10^5$, the vane boundary layers were visualized by painting the vanes with an emulsion of benzene, petroleum and aluminum oxide powder.

In April, 1964, measurements on the same cascade (with turbulence type 1) were made by H.H. Hebbel for the case of /11

TABLE 3[1]: MEASUREMENT PROGRAM FOR COMPRESSIBLE FLOW

Profile	NACA 65-608 NACA 65-612
Spacing ratio t/l	1.0
Vane angle β_S	130°
Reynolds number Re_1	1×10^5 4×10^5
Mach number Ma_1	0.3 to 0.9
Oncoming flow angle β_1	130° 135° 140° 145° 148°
Type of turbulence	1 2 3
Working plane position e/l	0.5

incompressible flow over the entire operating range. These measurements, in which the boundary layer was sucked off on the bottom walls, were preliminary experiments to [2]. From these it should be determined how the operating range of the cascade changes in comparison to[3], since for the measurements reported in[3] only adjustable baffle plates were available instead of suction. These measurements will be compared in this report, since so far they have not been evaluated in any report.

1. Tables 1 and 2 appear at the end of the article.

TABLE 4: MEASUREMENT PROGRAM FOR INCOMPRESSIBLE FLOW /12

Profile	NACA 65-608 NACA 65-612
Spacing ratio t/l	1.0
Vane angle β_S	130°
Reynolds number Re_1	1×10^5 2×10^5
Dynamic pressure q_1	39 mm H_2O 157 mm H_2O
Mach number Ma_1	0.08 0.15
Oncoming flow angle β_1	130? - 150°
Type of turbulence	1(Tu ≃ 0.3%)
Working plane position e/l	0.5

4. Evaluation of Measurements

4.1 Wake Measurement

The wake measurement for incompressible and compressible flow were evaluated according to the momentum method outlined by N. Scholz [8] for flat incompressible cascade flow. This method basically consists of using a momentum theorem to convert the flow in the wake working plane to a homogeneous outflow (cf. Fig.1). As shown by G. Kynast [9], the method may also be used for compressible flows, because the equalizing of the wake flow to a

homogeneous flow generally takes place with an insignificantly small density change. In order to use this method on compressor cascades the following variables must be measured along a wane spacing (from u to u + t, Fig. 1). /13

Measuring point coordinate	u
Dynamic pressure of the oncoming flow	$q_1 = p_{o1} - p_1$
Local total pressure loss	$\Delta p_o(u) = p_{o1} - p_{o2}(u)$
Local static pressure difference	$\Delta p(u) = p_2(u) - p_1$
Local outflow angle	$\beta_2(u)$

Using the Scholz method presupposes that the wake depressions of the individual vanes are still separate from one another, but that the static pressure $p_2(2)$ over the vane spacing is already nearly constant. Both requirements can be fulfilled by setting the wake measurement plane a suitable distance away (e/l), except if the flow on the vane is very strongly separated. It has also been shown that it is sufficient to determine the local outflow angle $\beta_2(u)$ as the arithemetic mean value of a fewmmeasured values of $\beta_2(u)$ outside the loss depression. There the gradient of $p_2(u)$ in the u direction is zero. This has been amply confirmed by numerous measurements (cf. also [8]).

The results of the wake measurement give the following aerodynamic coefficients for flat compressor cascades according to [8]:

loss coefficient:
$$\zeta_{V1} = \frac{p_{o1} - p_{o2}}{q_1} = G - K \qquad (1)$$

pressure shift:
$$\frac{\Delta p}{q_1} = \frac{p_2 - p_1}{q_1} = P + 2K \sin^2 \beta_{2m} \qquad (2)$$

dynamic pressure of outflow: $$\frac{q_2}{q_1} = 1 - \zeta_{V1} - \frac{\Delta p}{q_1} \qquad (3)$$

outflow angle: $$\cot \beta_2 = \left[1 + \frac{K}{1-G-P}\right] \cdot \cot \beta_{2m} \qquad (4)$$

flow deflection: $$\Delta\beta = \beta_1 - \beta_2 \qquad (5)$$ /14

The following abbreviations are used in these equations:

Mean value of the local total pressure loss:

$$G = \frac{1}{t} \int_u^{u+t} \frac{p_{o1} - p_{o2}(u)}{q_1} \, du \qquad (6)$$

Mean value of the local static pressure difference:

$$P = \frac{1}{t} \int_u^{u+t} \frac{p_2(u) - p_1}{q_1} \, du \qquad (7)$$

Scholz correction:

$$K = \frac{1}{t} \int_u^{u+t} \frac{q_2(u)}{q_1} \, du - \left[\frac{1}{t} \int_u^{u+t} \sqrt{\frac{q_2(u)}{q_1}} \, du\right]^2 \qquad (8)$$

Mean outflow angle in the wake measurement plane:

$$\beta_{2m} = \frac{1}{n} \cdot \sum_n \beta_2(u) \qquad (9)$$

All coefficients are related to the dynamic pressure $q_1 = p_{o1} - p_1$ of the oncoming flow. Eq. (8) was evaluated according to the method given in [8]. For the formation of sums in Eqs. (6) and (7) the weights g_ν as per Eltermann [10] were calculated with the following formulas for nonequidistant support points u_ν and quadratic interpolation:

$$g_\nu = \frac{1}{6} \cdot \left[- h_{\nu-1} + 3\, h_\nu + 3\, h_{\nu+1} - h_{\nu+2} \right] \quad ; \quad \nu \text{ uneven}$$

$$g_\nu = \frac{1}{6} \cdot \left[4\, h_\nu + 4\, h_{\nu+1} \right] \quad ; \quad \nu \text{ even}$$

$$\nu = 1, 2, 3, \ldots, 2n + 1 \quad ; \quad n \text{ integer} \qquad (10)$$

$$h_\nu = u_\nu - u_{\nu-1}$$

The total number of measurement points must be uneven if the integration weights as per Eq. (10) are calculated. /15

For incompressible flow, $c_{N1} = N/q_1 \cdot \ell$ was also calculated in addition to the normal force coefficient. (N = normal force per unit length of the vane, acting perpendicular to the chord.) The weight measurement gives the following:

$$c_{N1} = \left[c_A \cdot \cos \alpha_\infty + c_W \cdot \sin \alpha_\infty \right] \cdot \frac{\sin^2 \beta_1}{\sin^2 \beta_\infty} \qquad (11)$$

with $\alpha_\infty = \beta_\infty - \beta_S$,

$$\cot \beta_\infty = \frac{1}{2} (\cot \beta_1 + \cot \beta_2) \quad ,$$

$$c_A = 2 \cdot \frac{t}{\ell} \cdot (\cot \beta_2 - \cot \beta_1) \cdot \sin \beta_\infty + \frac{t}{\ell} \cdot \zeta_{V1} \cdot \frac{\sin^2 \beta_\infty}{\sin^2 \beta_1} \cdot \cos \beta_\infty$$

and $$c_W = \frac{t}{\ell} \cdot \zeta_{V1} \cdot \frac{\sin^3 \beta_\infty}{\sin^2 \beta_1}$$

4.2 Pressure Distribution

The local static pressure p(x) on the vane contour is measured against the static pressure p_1 of the oncoming flow and divided by the dynamic pressure of the oncoming flow $q_1 = p_{o1} - p_1$. The resulting pressure coefficient

$$c_{p1} = \frac{p(x) - p_1}{q_1} \qquad (12)$$

is plotted over the profile depth x/l referred to.

By integrating the pressure distribution we can calculate in an approximate manner the normal force coefficient c_{N1} of the cascade if we ignore the frictional force on the vane surface. With the flow under consideration this can be done without any hesitation because then the frictional force is directed almost parallel to the profile chord. Then according to [8] the normal force coefficient turns out to be:

$$c_{N1} = \oint c_{p1}\, d\left(\frac{x}{l}\right) = \sum_{\nu} (c_{p1})_{\nu} \cdot g_{\nu} \qquad (13)$$

The coefficient c_{N1} is given with the correct sign (positive, ?/16 if N points in the positive y direction), if the pressure distribution on the pressure side is progressively integrated in the positive x direction and on the suction side in the negative x direction. Eq. (13) is evaluated numerically according to Eq. Eq. (10).

4.3 Jet Contraction

The growth of the side wall boundary layers in the flow direction within the vane grid results in the fact that even in the cross-section the two-dimensional continuity equation is no longer satisfied; instead the mass flow density increases there. This deviation from flat flow is expressed by the contraction coefficient

$$\mu = \frac{\varrho_2\, w_{2a}}{\varrho_1\, w_{1a}} = \frac{\varrho_2\, w_2 \sin \beta_2}{\varrho_1\, w_1 \sin \beta_1} \qquad (14)$$

in the compressible case. In this equation the angles β_1 and β_2 are known directly from the wake measurement; the relationship of the densities and velocities can be calculated as follows from

the results of the wake measurements [11]:

$$\frac{\varrho_2}{\varrho_1} = \pi^{\frac{1}{\varkappa}} \cdot \pi_o^{\frac{\varkappa-1}{\varkappa}} \tag{15}$$

$$\frac{w_2}{w_1} = \sqrt{1 + \frac{\pi_o^{\frac{\varkappa-1}{\varkappa}} - \pi^{\frac{\varkappa-1}{\varkappa}}}{\frac{\varkappa-1}{2} \mathrm{Ma}_1^2 \cdot \pi_o^{\frac{\varkappa-1}{\varkappa}}}} \tag{16}$$

For the sake of brevity, the pressure ratio π and the loss factor π_o (also called the throttle factor) are introduced into Eqs. (15) and (16). They are obtained from the wake measurement results:

$$\pi = \frac{p_2}{p_1} = 1 + \frac{\Delta p}{q_1} \cdot \left[\left(1 + \frac{\varkappa-1}{2} \mathrm{Ma}_1^2\right)^{\frac{\varkappa}{\varkappa-1}} - 1 \right] \tag{17}$$

$$\pi_o = \frac{p_{o2}}{p_{o1}} = 1 - \zeta_{V1} \cdot \left[1 - \frac{1}{\left(1 + \frac{\varkappa-1}{2} \mathrm{Ma}_1^2\right)^{\frac{\varkappa}{\varkappa-1}}} \right] \tag{18}$$

#17

With Eqs. (15) and (16), Eq. (14) for the contraction coefficient becomes:

$$\mu = \pi^{\frac{1}{\varkappa}} \cdot \pi_o^{\frac{\varkappa-1}{\varkappa}} \cdot \frac{\sin \beta_2}{\sin \beta_1} \cdot \sqrt{1 + \frac{\pi_o^{\frac{\varkappa-1}{\varkappa}} - \pi^{\frac{\varkappa-1}{\varkappa}}}{\frac{\varkappa-1}{2} \mathrm{Ma}_1^2 \cdot \pi_o^{\frac{\varkappa-1}{\varkappa}}}} \tag{14a}$$

The method given by N. Scholz [8] for correcting jet contraction was not used. The measured contraction coefficients are given.

4.4 Degree of Turbulence

The degree of turbulence is the relationship of the average turbulent velocity fluctuation to the mean flow velocity. As measurements by H.L. Dryden have shown, the fluctuations in all directions are the same size in wind tunnels at some distance behind the screensaand rectifiers, so that the degree of turbulence for the working section of a wind tunnel can simply beewritten as follows:

$$Tu = \frac{1}{w}\sqrt{\overline{w'^2}} \cdot 100 \ \% \qquad (19)$$

To determine this, a calibration curve $E_{cal} = f(w)$ is first plotted, and in so doing the temperature must be constant and therefore monitored with a thermoelement next to the hot-wire probe. The velocity w is measured with a Prandtl-tube. As per DISA, from the slope of the calibration curve the degree of turbulence turns out to be

$$Tu = \frac{E_{eff}}{w \cdot \frac{dE_{cal}}{dw}} \cdot 100 \ \% \qquad (20)$$

The potentials E_{eff} and E_{cal} are indicated by the anemometer.

5. Results of Preliminary Experiments with Incompressible Flow /18

In the cascade measurements by J. Bahr [3,4] no boundary layer suction was available on the working sections of the LST and HST. The static pressure p_{above} and p_{below} on the bottom walls was made equal to the static pressure p_1 on the side walls by adjusting movable baffle plates. After suction was installed, H.H. Hebbel carried out measurements on the NACA 65-608 and 65-612 compressor cascades with top and bottom suction in order to determine the effect of suction on the cascade flow, in partiuclarly the operating range. In so doing, the same vanes,

The same number of vanes in the cascade and the same weight probe were used as by J. Bahr. The Reynolds numbers used differ by about 20% or 10% and are shown in the figures. Only case 1 was studied.(smooth vanes, low degree of turbulence).

Fig. 5 shows the results of the wake measurements, namely the loss coefficient ζ_{V1}, the deflection $\Delta\beta$, the pressure shift $\Delta p/q_1$ and the contraction coefficient μ. The numerical values of these measurements with suction are listed in Table 5.

The loss coefficients measured by Bahr (dashed curve, without suction) and Hebbel (solid curve, with suction) agrees fairly satisfactorily in the left and central portion of the polar curves for the cascade. The fluctuations in this regionscan be attributed to the difference in Reynolds numbers, since precisely in this Reynolds number range the influence of the Reynolds number change is very large, as can be seen from Fig. 10. By contrast, the cascade polar curvesddiffer greatly from one another on the right branch. With suction, the loss increase first begins at greater oncoming flow angles, i.e. the useful oncoming flow angle regionsof the cascade (operating range) in increased by the suction.

Based on the measurement results for incompressible flow with suction (above and below), the five oncoming flow angles (β_1 = 130°, 135°, 140°, 145°, 148°) were determined for the experiments with compressible flow (also with suction).

The purpose of the preliminary experiments was to determine /19
the above five values for β_1. In addition, they offer the possibility of studying the effect of boundary layer suction on the cascade flow by comparison with Bahr's measurements. This will be done using the results of the wake and pressure distribution measurements.

The cascade polar curves (especially NACA 65-608) and also the pressure shift curve show that the jet contraction in the cascade has a noticeable effect on the vane boundary layers at higher vane loads. This becomes smaller with decreasing vane loadsand, moreover, in this case is covered by the effect of the Reynolds number change. Since the vane profiles studied are only slightly cambered ($c_A^* = 0.6$), "high vane load" in this case means a deflection of flow of about 15°-20°. In other words, the assumption made by Scholz [8], that the repercussion of jet contraction on the vane boundary layers is insignificantly small, applies in the case of compressor cascades only if the deflection of flow is not greater than about 10°-15°.

The flow deflection with suction was measured about 1° less than without suction, while the pressure shift was measured larger with suction. With planar flow, however, a smaller deflection also corresponds to a smaller pressure shift (as long as $\beta_2 > 90°$). From this it follows that at least the cascade flow without suction studied by Bahr was not two-di dimensional. It also follows from the equations for the Scholz jet contraction correction [8] that as a result of contracted flow the pressure shift drops, but the deflection increases. For example, the following equation is valid for the outflow angle:

$$\cot \beta_{2eben} = \mu_A \cdot \cot \beta_2$$

with μ_A = outflow contraction ($\mu_A > 1$), i.e. in planar flow $\cot \beta_2$ and β_2 are larger and the deflection $\beta_1-\beta_2$ is smaller. Likewise, the differences in the pressure shift, which rise sharply with large oncoming flow angles are to be attributed to contraction of the jet.

The contraction coefficient μ curve with and without suction /20 is plotted in Fig. 5. The jet contraction effect further results from the pressure distributions which are plotted for

the NACA 65-608 cascade in Figs. 6 and 7 and for 65-612 in Figs. 8 and 9. The pressure distributions are valid for $Re_1 = 1 \times 10^5$ and 1.2×10^5 respectively. The pressure distributions for $Re_2 = 2 \times 10^5$ do not contribute anything new with respect to jet contraction. Therefore, each figure shows only one pressure distribution for $Re_1 = 2 \times 10^5$ in order to keep the graphs as clear as possible. (On the pressure side of the vanes the pressure distributions for $Re_1 = 1 \times 10^5$ and 2×10^5 coincide.) We see that with the cascade flow without suction the velocity level on the vanes is considerably increased as a result of jet contraction and that even in the outflow (curve plotted at $x/l = 1$) the same pressure increase is not obtained as with suction.

The contraction coefficients μ for the measurements without suction plotted in Fig. 5 are not given in [4], but they can easily be calculated from the results of the wake measurements. Comparison of the contraction coefficients between the measurements with and without suction in Fig. 5 shows how strong the flow in the middle of the cascade is accelerated if the boundary layers on the four walls are not sucked off.

The claim made in [3] and [4] that the jet contraction due to the absence of suction is insignificant, is thus not true. A numerical example may suffice to explain this:

Cascade dimensions:

NACA 65-612
$t/l = 1$
$\beta_S = 130^\circ$
$\beta_1 = 140^\circ$

cf. Fig. 5, lower row of diagrams

Reynolds numbers: $Re_1 = 2{,}2 \cdot 10^5$

Mach number: $Ma_1 = 0{,}15$

For this cascade flow the following measurements were made by Bahr [4], (first row of figures in the following table):

	ζ_{V1}	$\Delta p/q_1$	$\Delta\beta$	μ
Measured values from [4]	0,0159	0,2493	13,1°	1,066
Corrected values	0,0142	0,3397	12,9°	0,997

For the correction as per [8], the value of the contraction function was assumed to be , i.e. 90% of the total jet contraction takes place between plane "1" and the plane of the center of life of the profile. The corrected values must give the contraction coefficient $\mu = 1$, which is also the case within the limits of rounding off error.

Although in the example chosen the deflection and contraction coefficient are relatively small, the correction gives a change in the loss coefficient of 11% and in the pressure shift of 36% (with respect to the measured values). The differences cannot be termed insignificant. Another question, to be sure, is whether the coefficients (ζ_{V1}, $\Delta p/q_1$, $\Delta\beta$) calculated by the correction can also be realized in a two-dimensional flow, expecially with strong deflection.

In opposition to this numerical example is Table 1 in [4], page 9, in which measured values and corrected values are also compared. The corrected values given there for ζ_{V1} and $\Delta p/q_1$ are wrong. Moreover, the correction does not apply to the outflow angle. If, as a check, we calculate the new contraction coefficient from the corrected values in [4] including the corrected outflow angle, we do not obtain $\mu = 1$, as is required, but $\mu \approx 1.07$, i.e. almost the same result as from the measured values.

The curves for μ in Figs. 5 and 28 show that with compressor cascades with more than 10°-15° deflection a two-dimensional flow without suction on all sides cannot be achieved. Whether with smaller deflections the measured coefficients correspond to those

for planar flow, must be checked by measurements with boundary layer suction on all sides.

Besides the contraction coefficient, a measure of the two- /22
dimensionality of cascade flow is the difference between the normal force coefficients c_{N1} which can be calcualted from the wake and pressure distribution measurements. In the case of adjacent flow, this difference (within the limits of measurement accuracy) must be zero if the flow is two-dimensional. The c_{N1} values in Table 5 already at $\beta_1 = 140°$ a difference of about 10°, while the values for μ are around 1.02 here. If we do not want to attribute this contradiction exclusively to measurement error, then only jet measurements over an extended range behind the cascade can provide information on how far the flow is three-dimensional.

After this manuscript was finished a paper appeared by Heilmann [12] in which detailed experimental and boundary layer theory studies are described on the effect of jet contraction on cascade flow.

6. Results for Compressible Flow

6.1 Summary of a Few Results from [2]

Before discussing the results of the measurements over the entire oncoming flow angle range, we will once more briefly give the most important results from [2]. These are shown in Fig. 10. Hebbel [2] studied only one oncoming flow angle in the middle of the operating range. Fig. 10 shows the influence of the degree of turbulence (case 2) and the surface roughness (turbulent thread and sand roughness, cases 3 and 4) on compressible flow due to a NACA 65-612 compressor cascade at different Reynolds numbers. The oncoming flow angles studied, $\beta_1 = 140°$, lies in the middle of the operating range, i.e. the flow is completely adjacent at high Reynolds numbers. The mach number is $Ma_1 = 0.5$ and the flow on the profile is therefore subcritical.

Fig. 10 shows that in case 1 (smooth vanes, low degree of turbulence) the loss coefficient of the cascade below a certain Reynolds number rises sharply. Connected with this is a simultaneous drop in deflection and pressure shift. The reason for /23
this is the appearance of locally limited separations of the laminary boundary layer (separation bubbles) on the profile. The appearance of the separation bubbles can be shifted to smaller Reynolds numbers both by increasing the degree of turbulence of the oncoming flow and by increasing the roughness on the profile. On the other hand, increasing the degree of turbulence or roughness causes the loss coefficient to rise in the region of high Reynolds numbers, because no separation bubbles appear there in case 1.

This report studies only the effect of increased turbulence in the entire operating range for both Reynolds numbers: $\bar{Re}_1 = 1 \times 10^5$ (appearance of laminar separation in case 1) and $Re_1 = 4 \times 10^5$ (adjacent flow in case 1). Case 4 (sand roughness) was not investigated further.

The results of the comprehensive measurements are summarized in tables 6 and 7.

6.2 Flow Loss

Low Reynolds Number

For the two compressor cascades studied, NACA 65-608 and NACA 65-612, the loss coefficient ζ_{V1} is plotted over the oncoming flow angle (cascade polar curves) in Figs. 11 and 12, and in Figs. 13 and 14 over the Mach number (transverse plot to the cascade polar curves). The upper diagrams in the figures are for the low Reynolds number $Re_1 = 1 \times 10^5$

The cascade polar curves in Figs. 11 and 12 shows that the

separation bubbles in case 1 (smooth vanes, low degree of turbulence) are more pronounced in the center of the operating range (smooth flow) than at the edges. With a jerky oncoming flow, the collecting point on the profile nose obviously counteracts the formation of separation bubbles. The polar curves also show that with the thicker profile the separation bubbles allow the loss to increase more sharply than with the thinner profiles. This can be easily explained, since the excess velocities on the profile and thus the necessary deceleration with the profile thickness increase. /24

By increasing the degree of turbulence (case 2) or by attaching a turbulence thread (case 3) the loss coefficient can be considerably reduced with respect to case 1 of normal cascade flow. At mach numbers Ma_1 = 0.3-0.7, this reduction (with respect to case 1) on a percentage basis is of the same order of magnitude and therefore, in absolute terms, greater at higher mach numbers, because here the loss is also greater. In the middle of the polar curves the loss reduction is greater than at the edges.

With profile NACA 65-608, cases 2 and 3 are about equivalent with respect to the loss reduction, while with profile NACA 65-612 in the lower mach number range, case 3 gives better results than case 2. From this it follows that both formthe magnitude of the degree of turbulence and also for the thickness and position of the turbulence thread there are optimum values which depend on the profile geometry and pressure distribution (pressure gradient, boundary layer thickness), but which were not present in these experiments.

This is also confirmed by the flow patterns shown in Fig. 15 ($Re_1 = 1 \times 10^5$, <u>incompressible</u> flow), which show that in cases 2 and 3 the separation bubbles are indeed reduced in size, but

they have not disappeared. According to these patterns, the result of increasing the degree of turbulence (case 2) is that the width of the separation bubble on the pressure side is reduced. In this connection the beginning of the bubble (point of separation) remains unchanged, while the end of the bubble (point of reattachment) on the profile migrates forward. This is the same effect which is observed when the Reynolds number is increased [2]. Thus, with respect to the laminar-turbulent transition, increasing the degree of turbulence increases the effective Reynolds number of the cascade. On the suction side, on the other hand, increasing the degree of turbulence surprisingly does not reduce the size of the separation bubble, but shifts it downstream, and indeed this shift is greater, the greater the oncoming flow angle. To be sure, this also reduces the flow loss, but not to the same degree as if the size of the separation bubble were reduced. It can also be seen that the range of oncoming flow angles in which the separation bubbles occur is narrowed down at a higher degree of turbulence. /25

For the turbulence thread on the suction side of the vanes (case 3), the flow patterns do not show any significant difference in comparison with case 1, although the measured losses differe considerably in the middle of the polar curves. Obviously the paint patterns on the vanes cannot always be produced with sufficient accuracy. On the one hand, gravity affects the distribution of the emulsion with the low dynamic pressures, and on the other hand the cascade flow is disturbed by the application of the emulsion and by the emulsion layer on the vanes. Yet the layer thickness is of the same order of magnitude as the turbulence thread, which in this case has a diameter of only 0.06 mm. We therefore suspect that the effectiveness of the turbulence thread on the emulsion-covered vane was cancelled by the emulsion. In comparing flow patterns and loss curves it must also not be forgotten that the flow patterns show only the length of the bubble, but not its thickness.

It is also evident from Figs. 11 and 12 that the polar curves for cases 2 and 3 deviate sharply from one another at the greatest oncoming flow angles and mach numbers ($Ma_1 = 0.7$). In case 3 the flow separates considerably earlier than in case 2. This can be explained by means of the pressure distribution shown in Figs. 23 and 27. Since with increasing Mach number the beginning of the bubble migrates upstream (also see [2]), the turbulence thread at these Mach numbers lies within the separation bubble or just in front of it in such a thick boundary layer that its effectiveness is cancelled. This effect could supposedly be prevented by selecting the turbulence thread so thick that the separation bubble disappears completely.

The phenomenon mentioned in the last paragraph also shows up in the graphs of the loss coefficient over the Mach number (Figs. 13 and 14). Here, too, the sharp increase in loss begins earlier in case 3 than in case 2, especially with large oncoming flow angles. On the other hand, the loss in case 3 is smaller as long as the flow has not yet separated. Thus in the range of subcritical flow, cases 2 and 3 are suitable for reducing the /26
loss, and in this connection case 3 (turbulence thread) is better. On the other hand, case 2 (high degree of turbulence) is better suited than case 3 for increasing the critical Mach number (i.e. Mach number of the incipient loss increase). It must be borne in mind, however, that this result can turn out differently if other values are chosen for the thickness of the turbulence thread or for the degree of turbulence.

High Reynolds Number

The lower diagrams in Figs. 11-14 show the measured losses for the Reynolds number $Re_1 = 4 \times 10^5$. Comparison of the two Reynolds numbers studied shows first of all that the loss level at $Re_1 = 4 \times 10^5$ is considerably lower. Separation bubbles are present on the profine not at all or only to a small

extent. Also compare this with Figu 10. Accordingly, the polar curves are flatter, especially with the thicker of the two profiles.

It is to be expected with high Reynolds numbers that both a turbulence thread on the profile, (case 3) and the increased degree of turbulence (case 2) will cause an additional flow loss with respect to normal flow (case 1). For the degree of turbulence this is confirmed by the measurements on the thicker profile. For the thinner profile, on the other hand, the polar curves for cases 1 and 2 overlap. With small and average oncoming flow angles the loss in case 2 is a little higher, and with large oncoming flow angles it is sometimes lower than in case 1. The accompanying pressure distributions do not give a sufficient explanation of this. Therefore, it is assumed that the collecting point on the profile nose plays a role. Perhaps the flow behind the collecting point can be more favorably slowed down at certain oncoming flow angles and mach numbers at a higher degree of turbulence, although even at lower degrees of turbulence the boundary layer is already turbulent. This is also in accordance with the fact that the increase in loss for large oncoming flow angles and large Mach numbers in cases 2 and 3 begin somewhat later than in casell.

For the turbulence thread (case 3) the increase in loss is smaller than expected. In places the differences between case 1 /27
& lie within the accuracy of measurement. However, even at this Reynolds number it could still not be determined if the loss at large oncoming flow angles is decreased by the turbulence thread. Evidently, at large oncoming flow angles the turbulence thread has a favorable effect on the turbulence boundary layers so that the friction loss within the boundary layer becomes smaller.

633 Flow Deflection

The measured deflections $\Delta\beta$ are plotted over the oncoming flow angle in Figs. 16 and 17 and the pressure shifts $\beta p/q_1$ are plotted in Figs. 18 and 19, also over the oncoming flow angle.

Low Reynolds Number

With the Reynolds number $Re_1 = 1 \times 10^5$, the pressure shift in cases 2 and 3 is significantly higher than in case 1, in accordance with the lower losses. In this connection, the difference with the thicker profile is considerably greater, so that the reduction in size of the separation bubbles also manifests itself here in an increase in deflection, while with the thinner profile differences in deflection are present only at high Mach numbers, where in fact the separation bubbles increase in size due to the Mach number influence. The additional loss caused by the laminar separation bubbles therefore primarily affects the static pressure shift, while it less strongly influences the deflection.

With respect to deflection and pressure shift, cases 2 and 3 are fairly equivalent; as with flow loss, with the exception of large oncoming flow angles with simultaneously high mach numbers. Here, especially with the thicker profile, case 2 (high degree of turbulence) is clearly the best. At high (i.e. supercritical) oncoming flowamach numbers and low Reynolds numbers, the increase in the degree of turbulence could be termed a suitable means for increasing the maximum lift.

High Reynolds Number /28

For the thinner profile at $Re_1 = 4 \times 10^5$ no differences appear in deflection and pressure shift, and only slight differences appear with the thicker profile.

6.4 Pressure Distributions

The pressure distributions for cascade NACA 65-608 are shown in Figs. 20-23 and those for cascade NACA 56-612 are shown in Figs. 24-27. At $x/l = 1$, the values $\beta p/q_1$ of the wake measurements are recorded in order to farily correctly infer the pressure distributions.

Low Reynolds Number

The pressure distributions, just like the loss and deflection, also differ significantly from one another in cases 1-3. The differences are greatest at high Mach numbers. The influence of the degree of turbulence and the turbulence thread can clearly be seen in the region of the separation bubbles, especially on the suction side. To a vast extent the pressure distribution is improved more by the increasedddegree of turbulence than by the turbulence thread. This is not in agreement with the fact that the turbulence thread often causes smaller losses than the increased degree of turbulence (for example, NACA 65-608; $\beta_1 = 145°$ at $Ma_1 = 0.3=0.6$). This strengthens the assumption mentioned in section 6.2 that in fact the turbulence thread reduces the friction loss in the boundary layer in many cases.

High Reynolds Number

Here the pressure distributions in cases 1-3 differ only slightly from one another. Even at $Re_1 = 4 \times 10^5$ faint separation bubbles are still present on the suction side and pressure side. Presumably these should be totally suppressed by a higher degree of turbulence or a thicker turbulence thread.

6.5 Jet Contraction /29

Because of the lakc of side wall suction it was not possible to influence the flow density ratio in the axial direction. Therefore a jet contraction deviating more or less from 1 was

present in the measurements. This is plotted in Figs 28 over the deflection $\Delta\beta$ for both compressor cascades studied and for both Reynolds numbers. Fig. 28 clearly shows that with compressor cascades the deflection of flow is crucial for the size of the contraction coefficient μ. By contrast, the effects of the Mach number, Reynolds, profile thickness and three types of turbulence on the contraction coefficient can be ignored.

A fairly two-dimensional flow with the two cascades exists only in the range of $\Delta\beta = 0°$ up to about 10° (this corresponds to a β_1 up to about 137°. However, since the contraction coefficient for the three types of turbulence studied are about equal, the results of cases 1-3 can be compared with one another without reservations.

The jet contraction is also the main reason why the curves $\Delta p/q_1$ over β_1 become horizontal earlier than the curves $\Delta\beta$ over β_1. Another reason for this is the loss already increases (right branch of polar curve) before the flow separates.

7. Summary

This report is concerned with the effect of an increased degree of turbulence and a profile turbulence thread on the compressible flow through two straight compressor cascades at different Reynolds numbers, mach numbers and oncoming flow angles.

The two compressor cascades consist of NACA 65-608 and NACA 65-612 vane profiles. The vane angle was $\beta_S = 130°$ and the spacing ration $t/l = 1$. The oncoming flow angle was varied from $\beta_1 = 130°$ to 148°, the Reynolds numbers were $Re_1 = 1 \times 10^5$ and 4×10^5, and the Mach numbers were between $Ma_1 = 0.3$ and 0.9.

The cascades were studied for the following three cases: /30

1) Smooth vanes, low degree of turbulence (0.2-1%)

2) Smooth vanes, high degree of turbulence (2.5-4.5%)

3) Vanes with turbulence threads (d = 0.06 mm) on the suction side (at $x/l = 0.25$), low degree of turbulence (0.2-1%).

The experiments included wake and pressure distribution measurements and formed the continuation of the studies begun in [2]. The strong influence of the Reynolds number on the action of the turbulence generator found in [2] was confirmed. Furthermore, it turns out that also the Mach number and especially the oncoming flow angle are important.

Low Reynolds Numbers, $Re_1 = 1 \times 10^5$

The reduction in profile loss in cases 2 and 3 as against case 1 is zero at oncoming flow angles close to the vane angle. It is greatest in the middle of the operating range of the cascade and falls off again at large oncoming flow angles. In this connection, case 3 (turbulence thread) is sometimes just as good as case 2 (high degree of turbulence) sometimes better.

In the range below the critical Mach number (i.e. the Mach number at which the loss coefficient suddenly increases) the relative decrease in the loss coefficient over the Mach number is fairly constant (for a fixed oncoming flow angle). Above the critical Mach number the separation of flow is shifted towards larger oncoming flow angles, and to be sure considerably more so in case 2 than in case 3.

Together with the drop in profile loss we obtain an increase in the pressure shift, and to a smaller extent also an increase in deflection. The effectiveness of the turbulence generator is more prominent with the thicker profile than with the thinner one.

High Reynolds Numbers, $Re_1 = 4 \times 10^5$

In all three cases the profile losses are without exception smaller than with $Re_1 = 1 \times 10^5$. As a result, in cases 2 and 3 the separation bubbles on the profile were only reduced in size at the lower Reynolds number but they were not entirely suppressed. This is confirmed by the pressure distribution.

At $Re_1 = 4 \times 10^5$ an additional loss frequently arises in cases 2 and 3, but this is small in comparision with the decrease in loss at $Re_1 = 1 \times 10^5$.

With large oncoming flow angles a drop in the loss coefficient can occur even at $Re_1 = 4 \times 10^5$ in cases 2 and 3, in particularly if at the same time the Mach number of the oncoming flow is high. It appears athat the friction resistance of the turbulent, compressible boundary layer can also be reduced in these cases by an increased degree of turbulence, but especially by the turbulence thread.

In the lightcoff preliminary experiments with incompressible flow, the importance of sucking off the boundary layer for the two-dimensionality of the cascade flow was also discussed.

REFERENCES

1. Hebbel, H.H., Über den Einfluss der Machzahl und der Reynoldszahl auf die aerodynamischen Beiwerte von Turbinenschaufelgittern bei verschiedener Turbulenz der Strömung.[Effect of Mach Number and Reynolds Number on the Aerodynamic Coefficients of Turbine Cascades for Different Degrees of Flow Turbulence], Dissertation, Braunschweig 1962, Forsch. Ing. -Wesen 30 /3, 65-77 (1964). /32

2. Hebbel, H.H.,"Effect of Mach Number and Reynolds Number on the aerodynamic coefficients of turbine cascades for different degrees of flow turbulence," Forsch. Ing.-Wesen, 33/5, 141-150 (1967).

3. Bahr, J., "Studies on the effect of profile thickness on compressible flat flow through compressor cascades," Dissertation Braunschweig, Forsch. Ing. -Wesen,30/11 11-25 (1964).

4. Bahr, J., "Studies on the effect of profile thickness on the flow through flat compressor cascades at high subsonic speeds. Part I: Studies on incompressible flow," DFL Report 089, Report 60/26 of the Aerodynamics Institute of the German Aeronautics and Space Research Center, Braunschweig.

5 Ackermann, E., Eichmessungen am kleinen Gitterwindkanal [Calibration measurements on Small Cascade Wind Tunnels] Report 56/17 of the Institute for Fluid Mechanics, Braunschweig Technische Hochschule.

6. Scholz, N and U. Hopkes, "The High speed cascade wind tunnel of the German Aeronautics Research Center, Braunschweig," Forsch. Ing.-Wesen 25/ 133-147 (1959).

7. Krux, P., Untersuchungen an Verdichterschaufelgittern mit verschiedenen Schaufelprofilen bei hohen Unterschallgeschwindigkeiten.[Studies on Compressor Cascades with Different Vane Profiles at High Subsonic Speeds] DFL Report 0313, Report 65/30 of the Institue for Aerodynamics of the German Aeronautics and Space Research Center, Braunschweig (1965).

8. Scholz, N., "Performing systematic measurements on flat cascades," Zeitschrift für Flugwissenschaften 4/10, 313-334, (1956).

9. Kynast, G., "Analyzing wake measurements for compressible flows through cascades," Zeitschrift für Flugwissenschaften 12/2, 69-71 (1964).

10. Eltermann; H., Numerical integration in the case of non-equidistant abscisses and calculation of curve integrals," ZAMM, 33/8-9, 254-255 (1953). /33

11. Scholz, H., "Formulas and tables for compressible cascade flows," Report 57/17 of the Institute for Fluid Mechanics, Braunschweig Technische Hochschule (1957).

12. Heilmann, W., Experimentelle und grenzschichttheoretische Untersuchungen an ebenen Verzögerungsgittern bei kompressibler Strömung insbesondere bein Änderung des axilaen Stromdichteverhältnisses und der Zuströmturbulenz, [Experimental and Boundary Layer Theory Studies on Flat Retardation Cascades with Compressible Flow, in Particular while Changing the Axial Flow Density Ratio and the Oncoming Flow Turbulence] DLR Research Report 67-88, German Aeronautics and Space Research Center, 1967.

LIST OF FIGURES

List of Tables

ORIGINAL PAGE IS
OF POOR QUALITY

Deutsche Forschungsanstalt für Luft- u. Raumfahrt (DFL) Institut für Aerodynamik

Markings on the flat compressor cascade

p. 36

Fig. 1

Bearbeitet Barsun | Datum 23. 5 1967 | Skizzenblatt Nr. | Bericht Nr 68 / 34

Deutsche Forschungsanstalt für Luft- u Raumfahrt (DFL) – Institut für Aerodynamik	Turbulence screen V and location of turb. screen in working section	p. 37
		Fig. 2

ⓐ Turbulenc screen V

scale 1:5

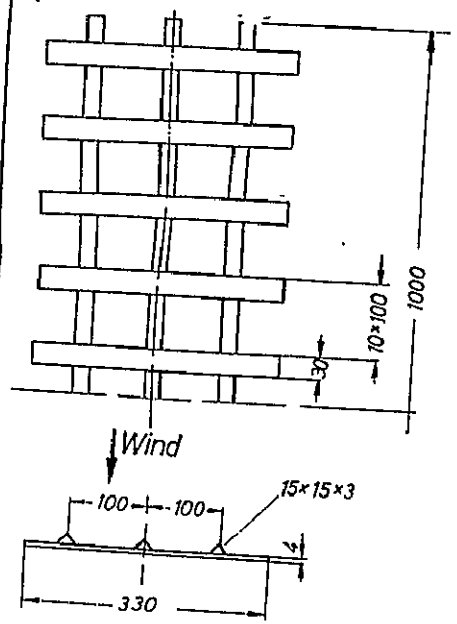

Geometric transmission = 55.5%

ⓑ Location of turbulence screen in working section

scale 1:10

Side view

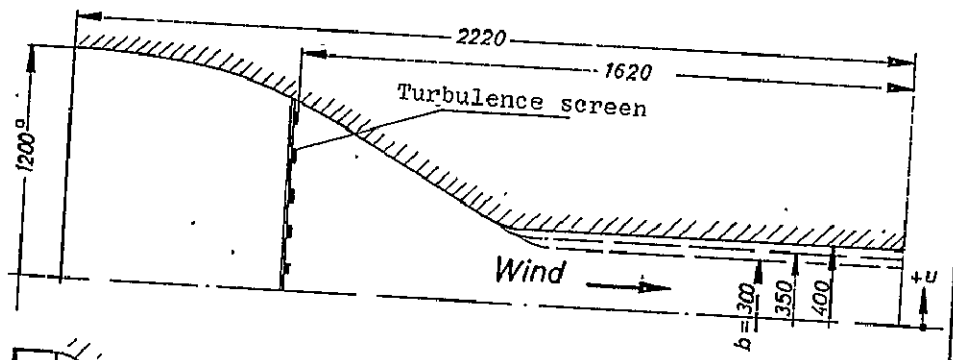

Top view

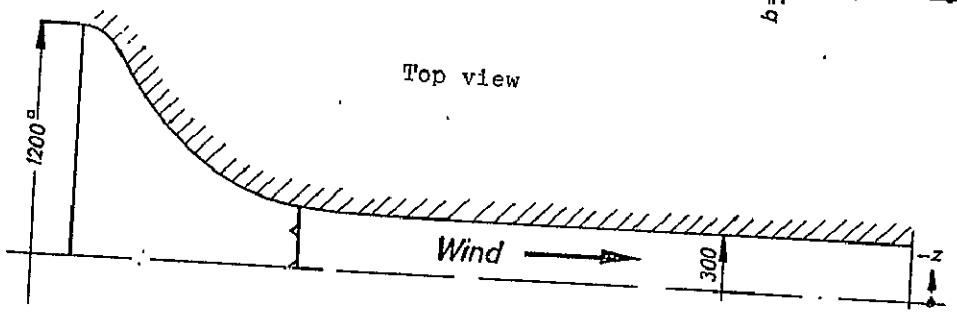

Bearbeitet: Barsun Franz	Datum: 14. 12 1966	Skizzenblatt Nr	68/34

Deutsche Forschungsanstalt für Luft- u. Raumfahrt (DFL) Institut für Aerodynamik	Degree of turbulence in the working section of the HST	p. 38
		Fig. 3

Turbulence screen as per Fig. 6 installed in the nozzle.
Height of working section 350 mm
Measured degree of turbulence values from [7]
Institute Report 65/30

Re_1 with respect to l = 60 mm

△	$Re_1 = 0{,}5 \cdot 10^5$
●	$Re_1 = 1 \cdot 10^5$
○	$Re_1 = 2 \cdot 10^5$
□	$Re_1 = 3 \cdot 10^5$
■	$Re_1 = 4 \cdot 10^5$

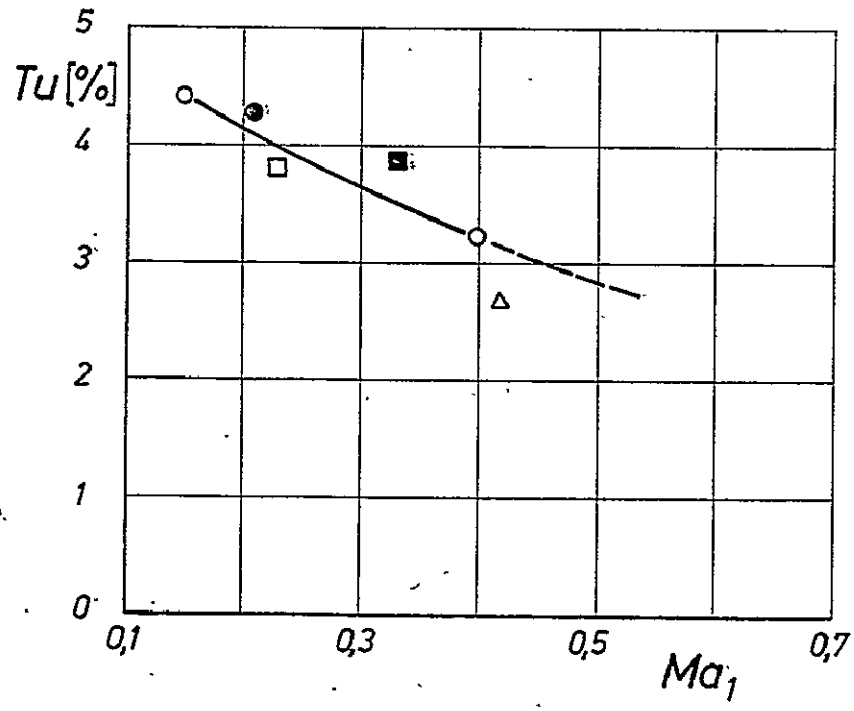

Deutsche Forschungsanstalt für Luft- u. Raumfahrt (DFL) Institut für Aerodynamik	Vane profile and grid arrangement studied	p. 39
		Fig. 4

ⓐ vane profile studied

NACA 65-608
(d/l = 0.08)

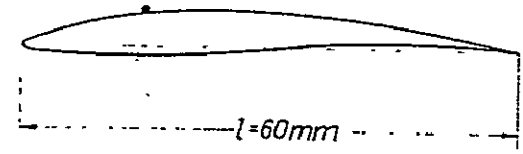

NACA 65-612
(d/l = 0.12)

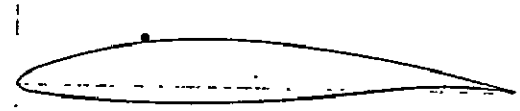

ⓑ grid arrangement studied
(here shown with Profile NACA 65-612)

t/l = 1.0
β_s = 130°
β_1 = 140°
e/l = 0.5

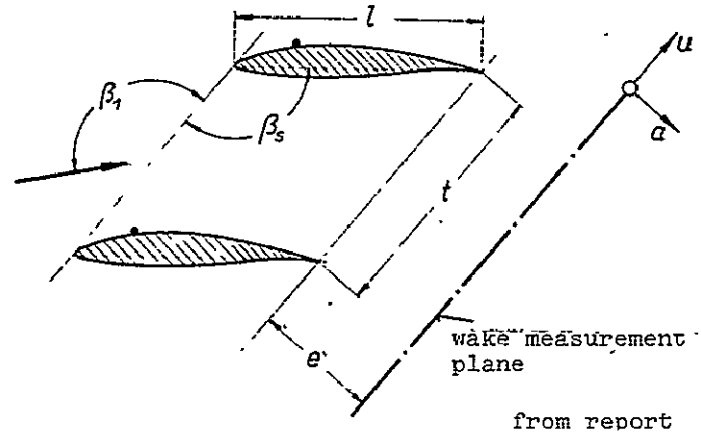

from report
65/5

Bearbeiter: Hebbel, Schuppe	Datum: 26.5.64	Skizzenblatt Nr.:	Bericht Nr.: 68/34

Wilhelm Fahrig, Braunschweig 10a2 1470

	measurements with suction top and bottom		measurementw without suction [3,4]	
$Re_1 =$	$1 \cdot 10^5$	$2 \cdot 10^5$	$1{,}2 \cdot 10^5$	$2{,}2 \cdot 10^5$
NACA 65-608	—□—	—■—	---□---	---■---
NACA 65-612	—◇—	—◆—	---◇---	---◆---

Deutsche Forschungsanstalt für Luft- u. Raumfahrt (DFL) Institut für Aerodynamik

Influence of bottom - wall suction on flow through comp. cascade

Dr. 40
Fig. 5

NACA 65-608
NACA 65-612

grid arrangement
$t/l = 1$
$\beta_s = 130°$
Mach numbers
$Ma_1 \approx 0{,}08$ und $0{,}15$
Type of turbulence
smooth vanes
$Tu_1 \approx 0{,}3\,\%$

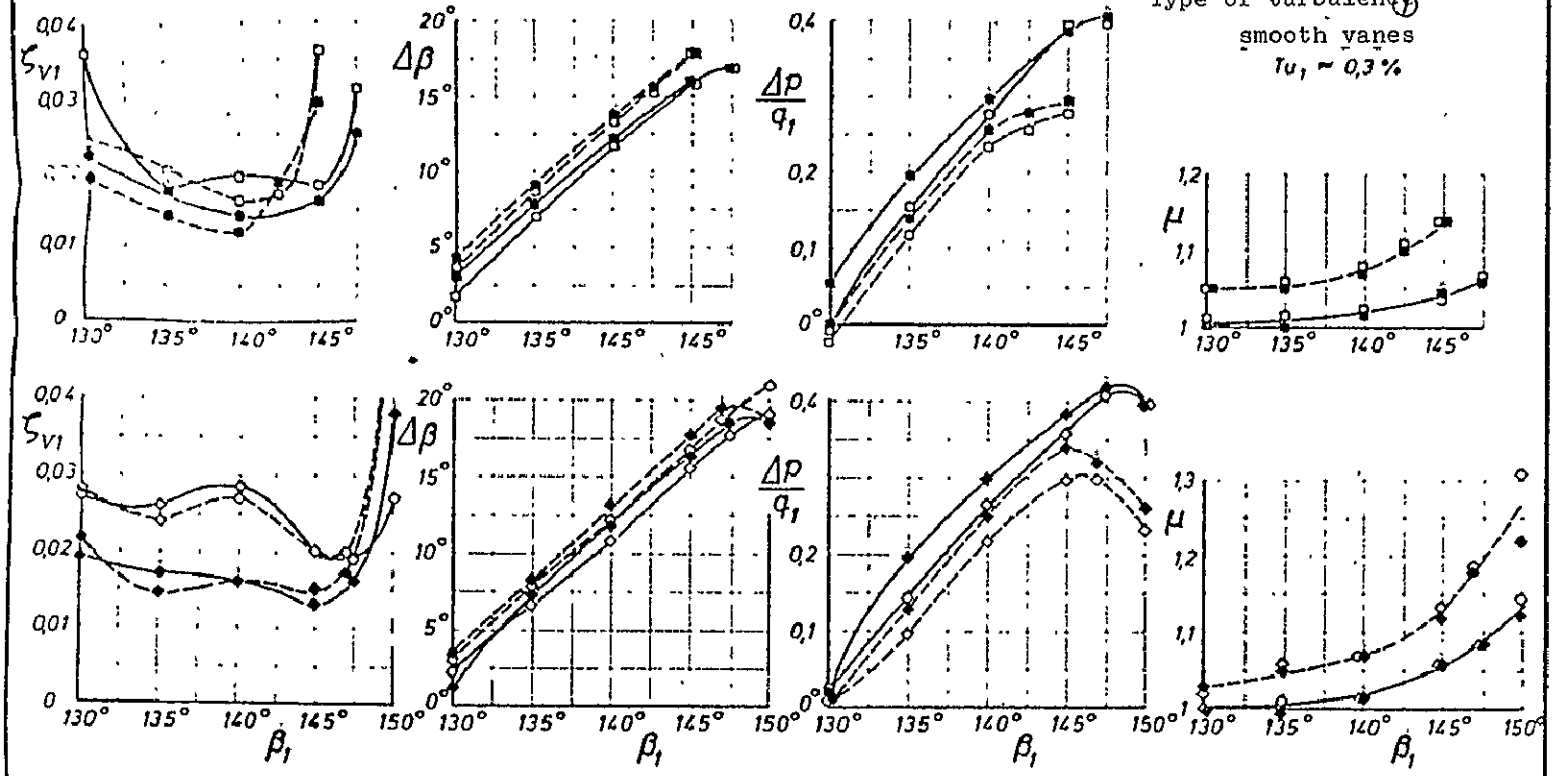

Bearbeitet	Datum	Zeichenblatt Nr.	Durchgang Nr.
Barsun Donner	18.3.68		68/34

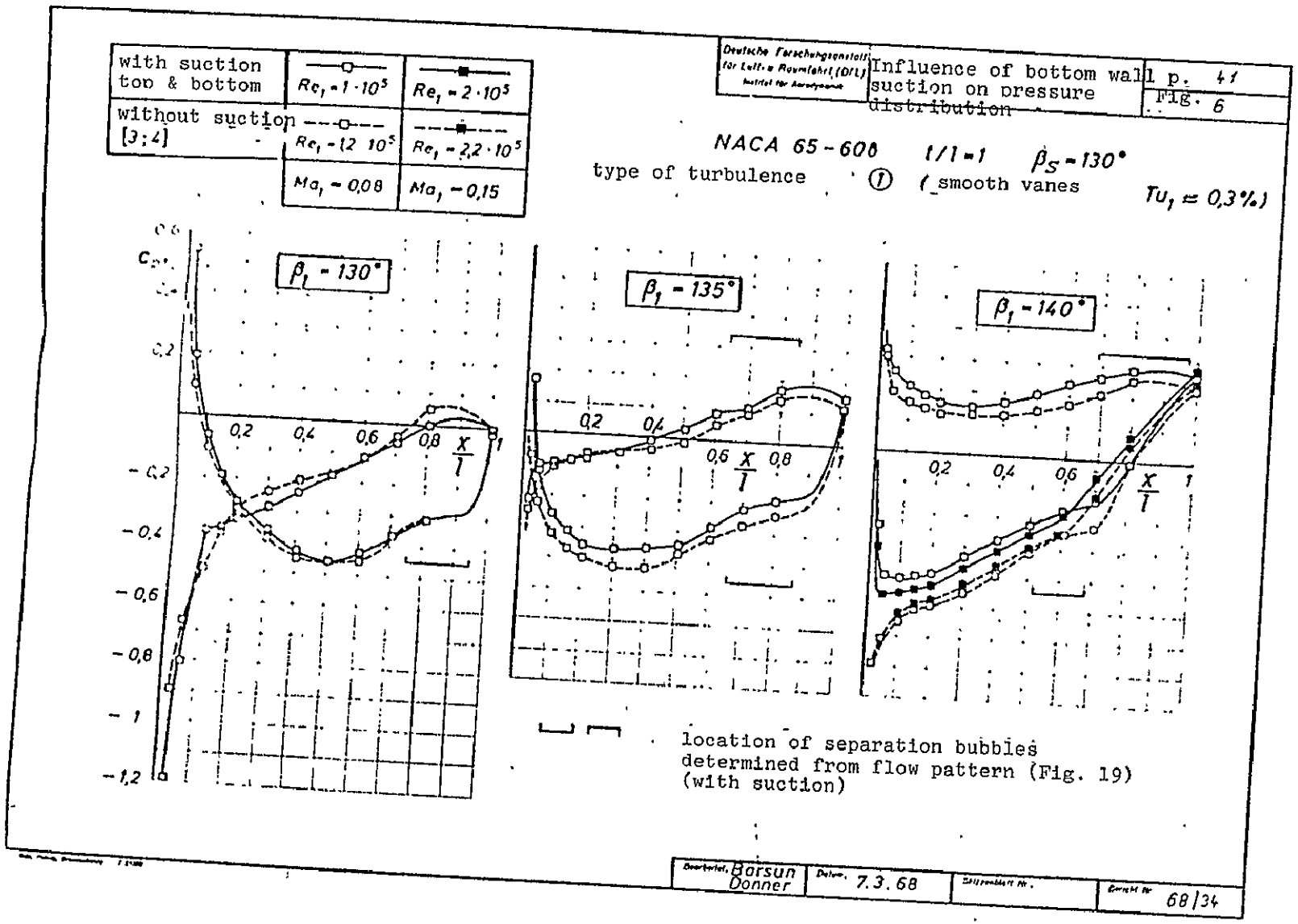
with suction top & bottom
$Re_1 = 1 \cdot 10^5$
$Re_1 = 2 \cdot 10^5$
without suction [3;4]
$Re_1 = 1.2 \cdot 10^5$
$Re_1 = 2.2 \cdot 10^5$
$Ma_1 = 0.08$
$Ma_1 = 0.15$
Deutsche Forschungsanstalt für Luft- und Raumfahrt (DFL) Institut für Aerodynamik
Influence of bottom wall suction on pressure distribution
p. 41
Fig. 6
NACA 65-606 t/l = 1 $\beta_S = 130°$
type of turbulence ① (smooth vanes $Tu_1 \approx 0.3\%$)
$\beta_1 = 130°$
$\beta_1 = 135°$
$\beta_1 = 140°$
c_p
0.2
-0.2
-0.4
-0.6
-0.8
-1
-1.2
0.2 0.4 0.6 0.8 1
$\frac{x}{l}$
location of separation bubbles determined from flow pattern (Fig. 19) (with suction)
Bearbeitet: Barsun Donner
Datum: 7.3.68
Zeichnungs Nr.
Bericht Nr. 68/34

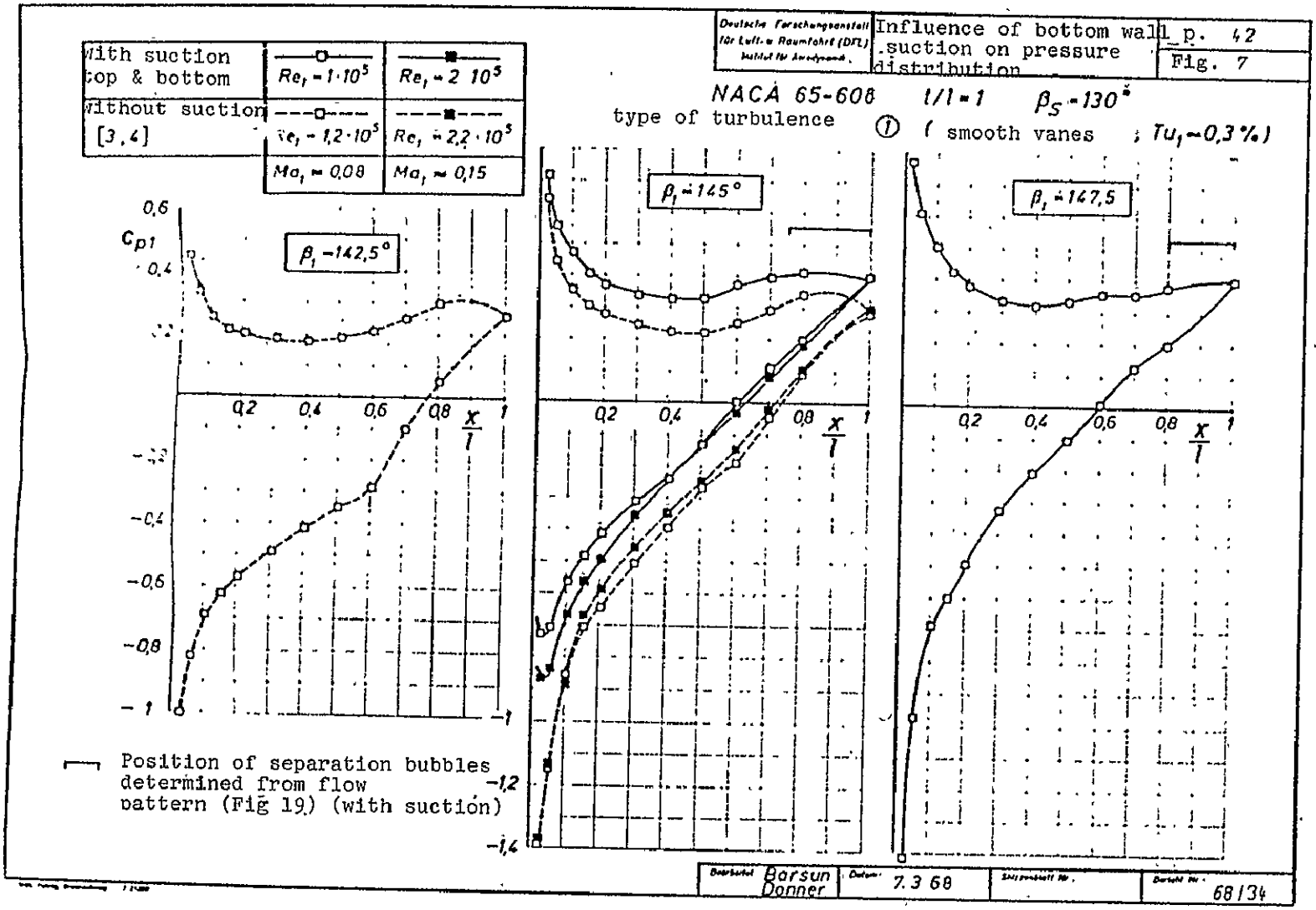

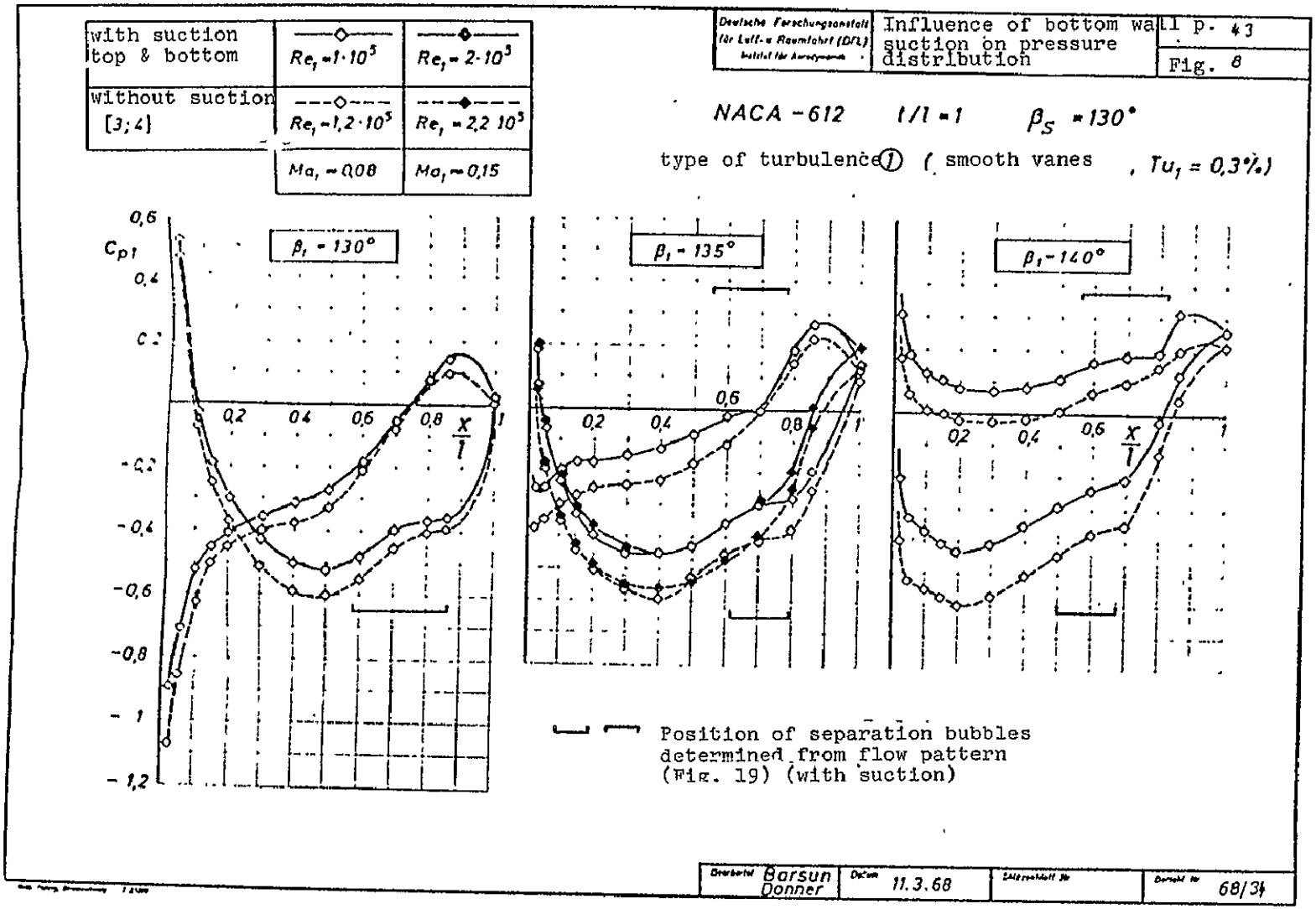
with suction top & bottom
Re1 = 1·10^5
Re1 = 2·10^5
without suction [3;4]
Re1 = 1,2·10^5
Re1 = 2,2·10^5
Ma1 = 0,08
Ma1 = 0,15
Deutsche Forschungsanstalt für Luft- u. Raumfahrt (DFL) Institut für Aerodynamik
Influence of bottom wall suction on pressure distribution
p. 43
Fig. 8
NACA - 612 l/l = 1 βS = 130°
type of turbulence ① (smooth vanes , Tu1 = 0,3%)
β1 = 130°
β1 = 135°
β1 = 140°
cp1
0,6
0,4
0,2
-0,2
-0,4
-0,6
-0,8
-1
-1,2
0,2
0,4
0,6
0,8
1
x/l
Position of separation bubbles determined from flow pattern (Fig. 19) (with suction)
Barsun Donner
11.3.68
68/34

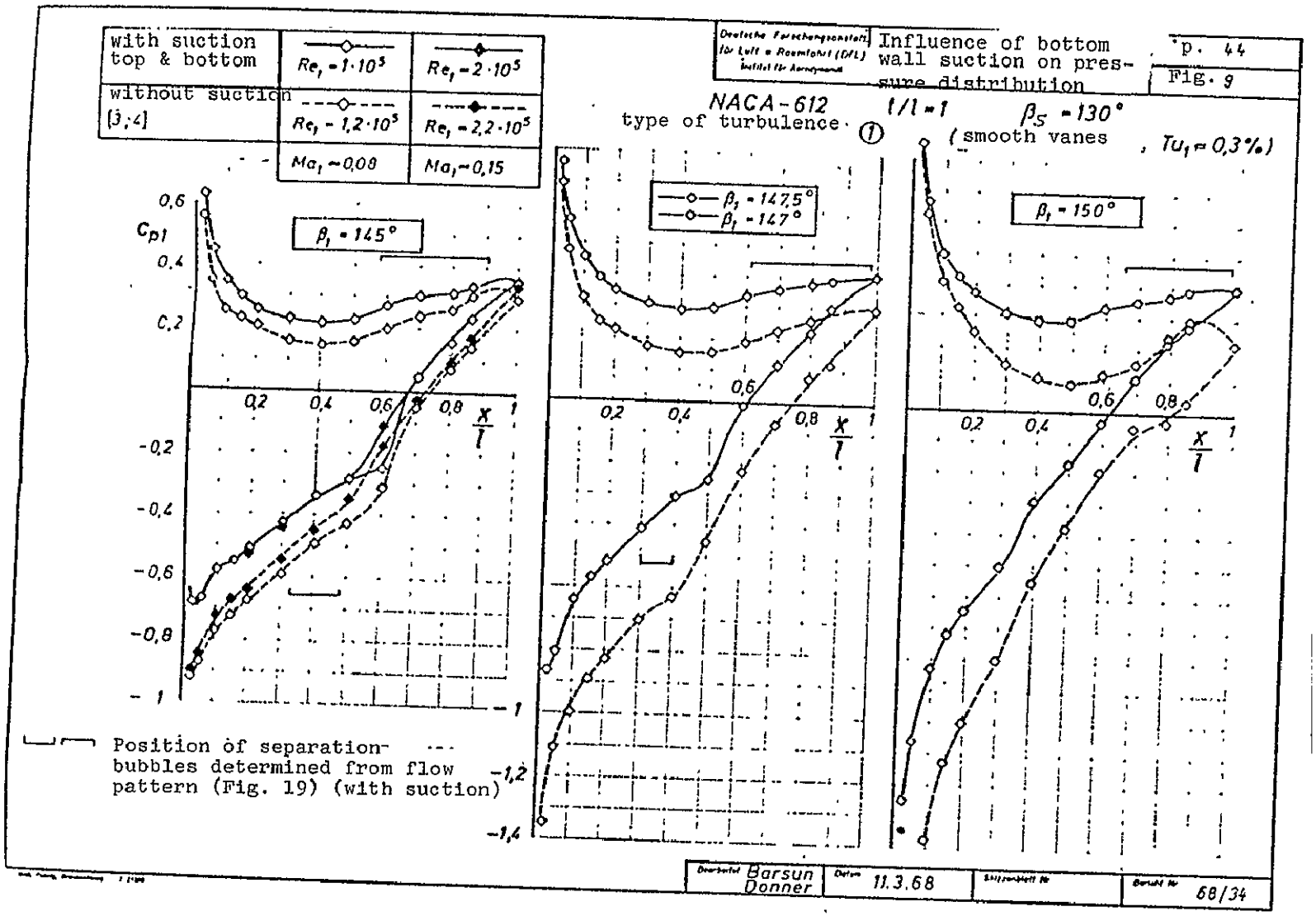

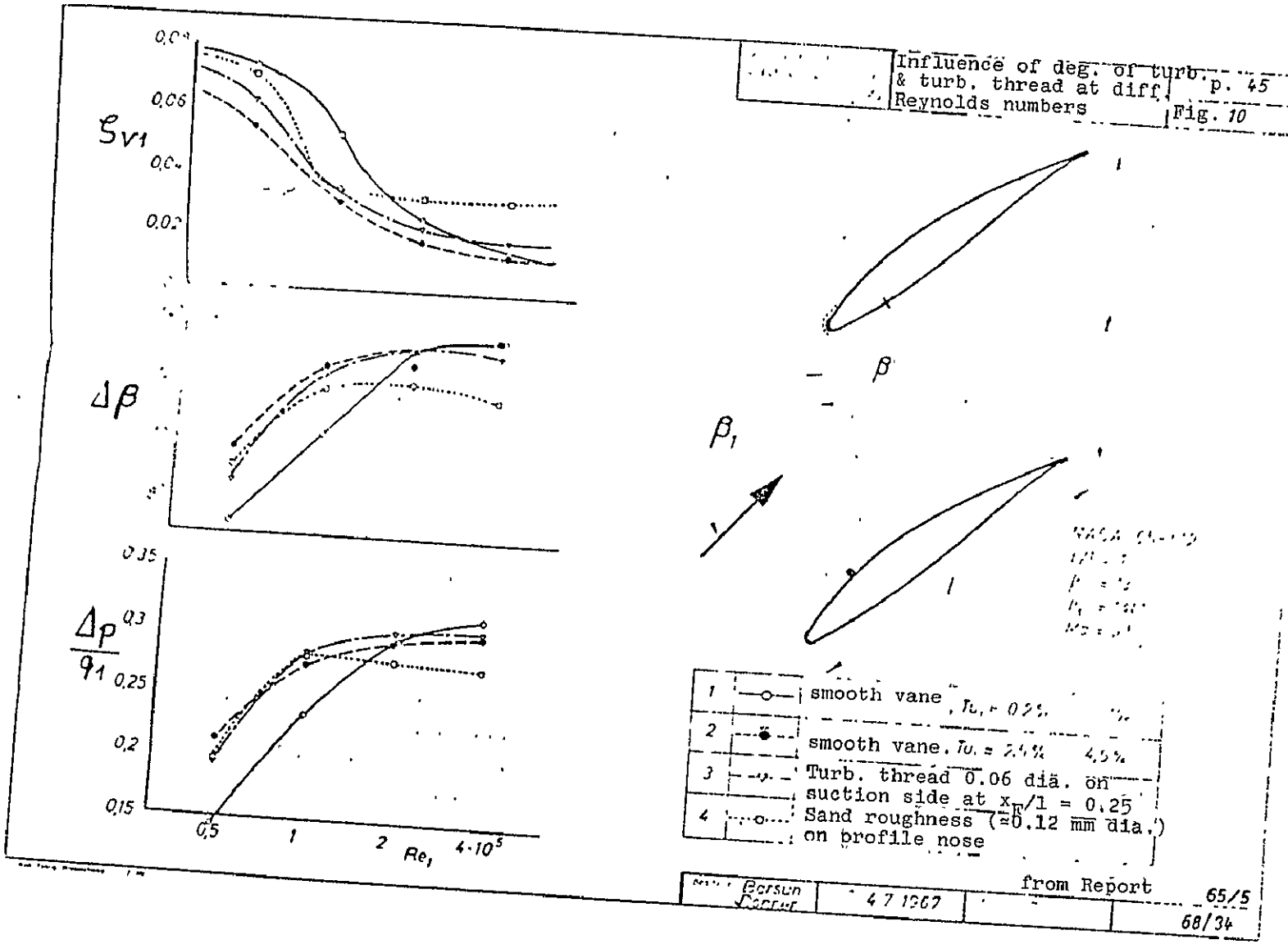
Influence of deg. of turb. & turb. thread at diff. Reynolds numbers
p. 45
Fig. 10
ζ_{v1}
0,06
0,02
$\Delta\beta$
$\frac{\Delta p}{q_1}$
0,3
0,25
0,2
0,15
0,5
1
2
Re_1
$4 \cdot 10^5$
β
β_1
1 smooth vane
2 smooth vane.
3 Turb. thread 0.06 diä. on suction side at $x_T/l = 0,25$
4 Sand roughness (≈0.12 mm dia.) on profile nose
from Report
65/5
68/34

ORIGINAL PAGE IS
OF POOR QUALITY

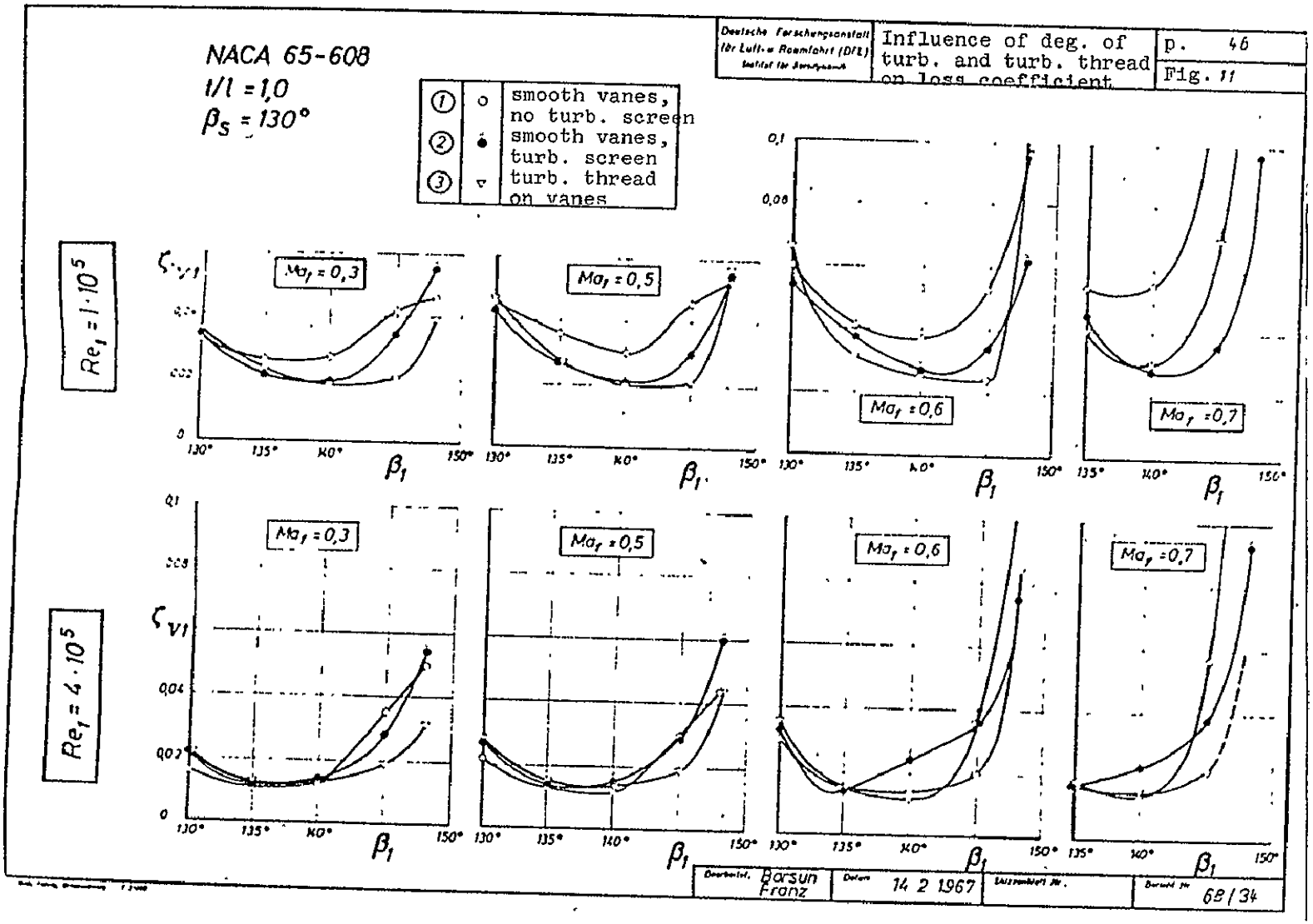

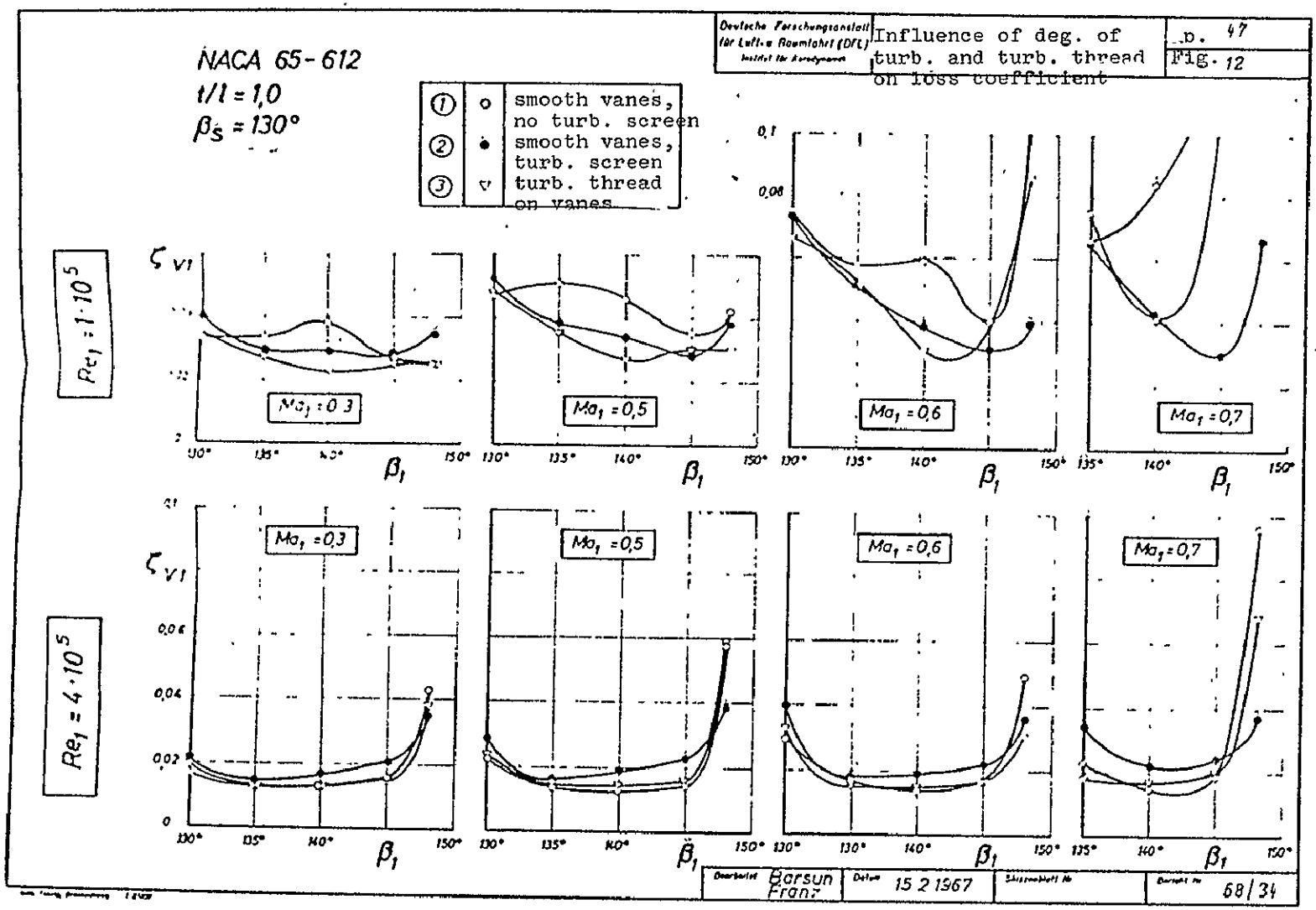
Deutsche Forschungsanstalt für Luft- u. Raumfahrt (DFL)
Institut für Aerodynamik
Influence of deg. of turb. and turb. thread on loss coefficient
p. 47
Fig. 12
NACA 65-612
t/l = 1,0
βS = 130°
① smooth vanes, no turb. screen
② smooth vanes, turb. screen
③ turb. thread on vanes
Re1 = 1·10^5
Re1 = 4·10^5
ζ v1
Ma1 = 0,3
Ma1 = 0,5
Ma1 = 0,6
Ma1 = 0,7
β1
Bearbeitet Garsun Franz
Datum 15 2 1967
68/34

Deutsche Forschungsanstalt für Luft- u. Raumfahrt (DFL) Institut für Aerodynamik

Influence of deg. of turb. and turb. thread on loss coefficient

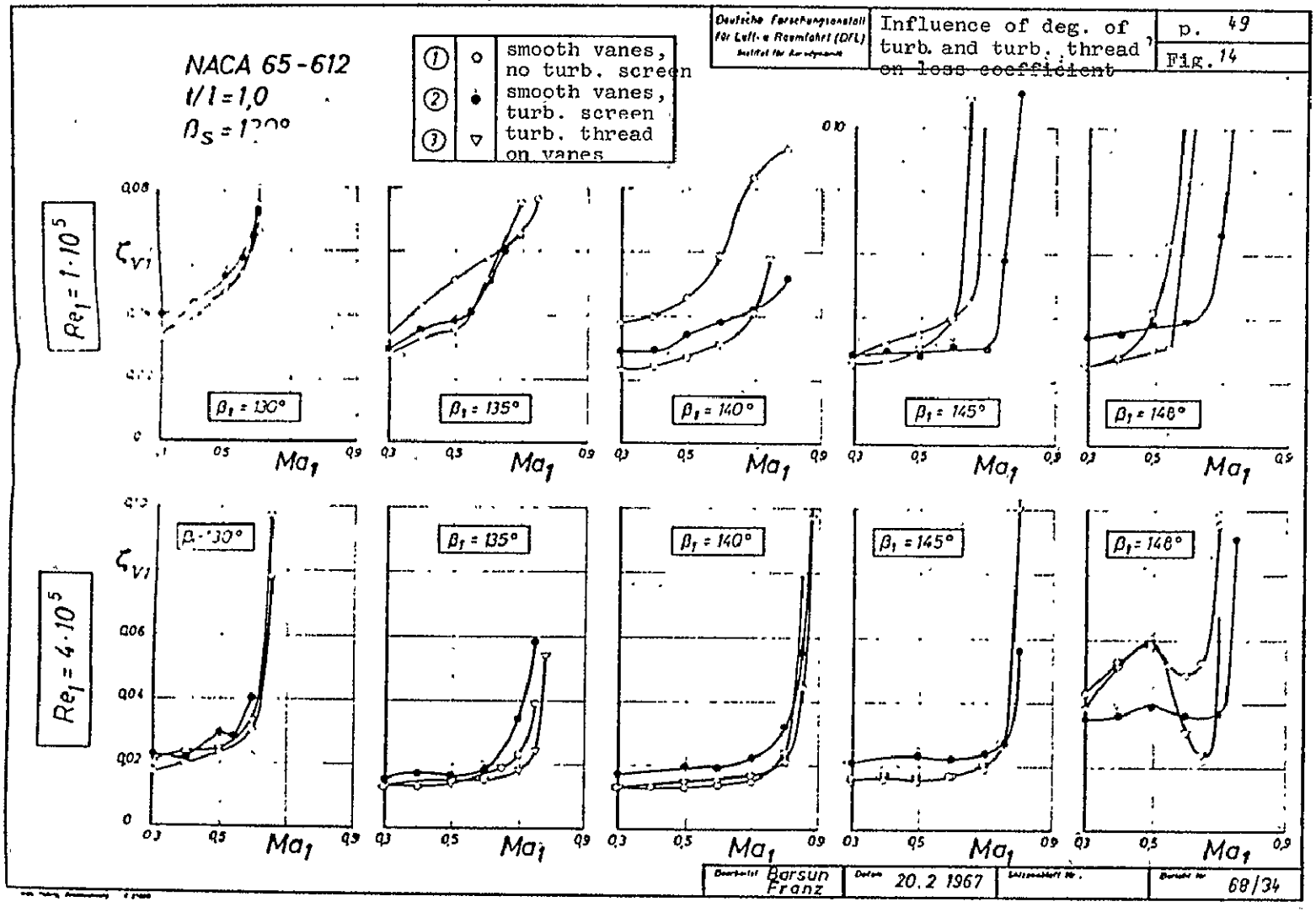

Bearbeitet Barsun Franz | Datum 20.2.1967 | Zeichnung Nr. | Bericht Nr. 68/34

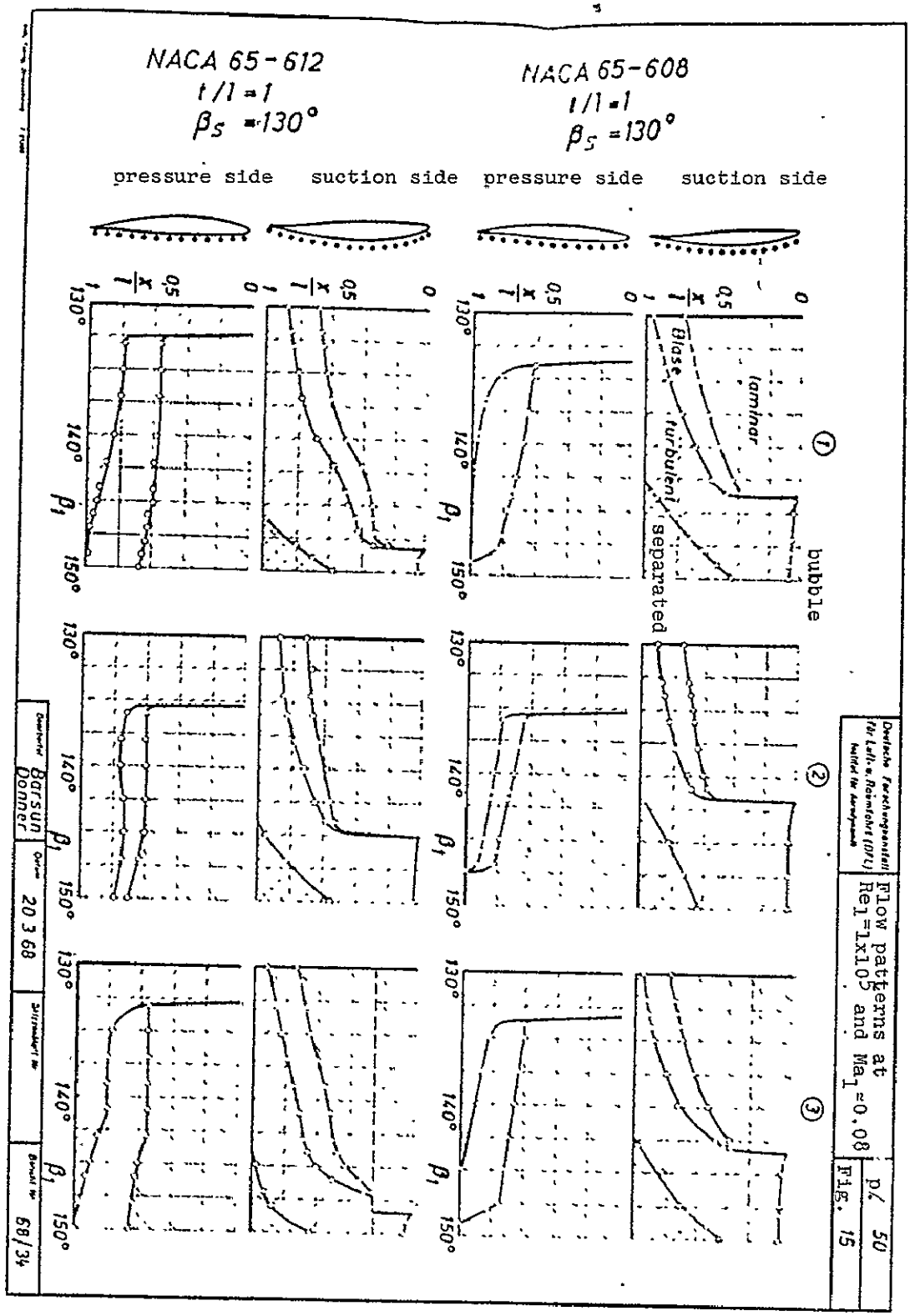

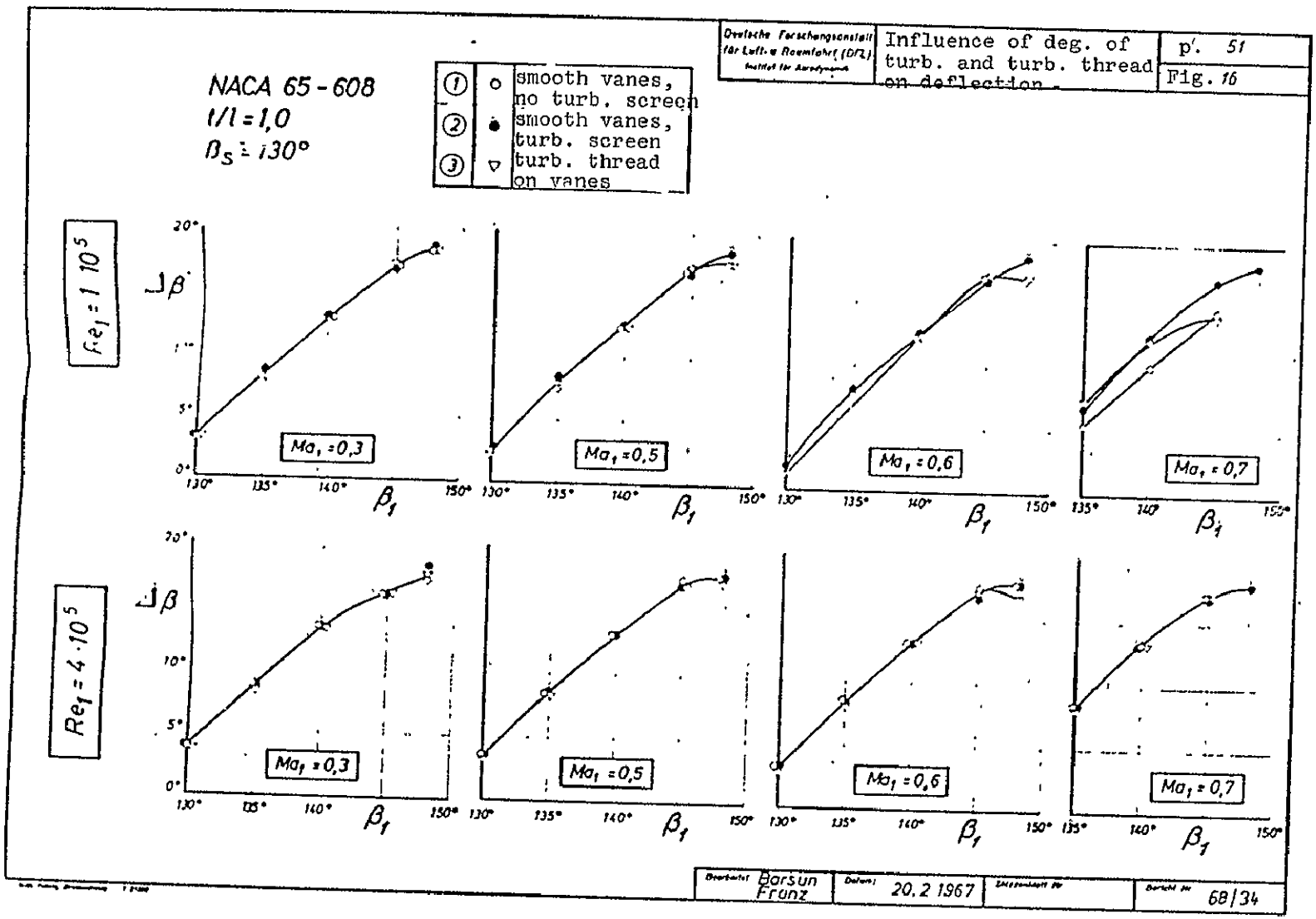
NACA 65 - 608
t/l = 1,0
$\beta_S \doteq 130°$
① smooth vanes, no turb. screen
② smooth vanes, turb. screen
③ turb. thread on vanes
Deutsche Forschungsanstalt für Luft- u. Raumfahrt (DFL) Institut für Aerodynamik
Influence of deg. of turb. and turb. thread on deflection
p. 51
Fig. 16
$Re_1 = 1 \cdot 10^5$
$Re_1 = 4 \cdot 10^5$
$\Delta\beta$
β_1
$Ma_1 = 0,3$
$Ma_1 = 0,5$
$Ma_1 = 0,6$
$Ma_1 = 0,7$
Bearb. Barsun Franz
Datum 20. 2 1967
Bericht Nr. 68/34

Deutsche Forschungsanstalt für Luft- u. Raumfahrt (DFL) Institut für Aerodynamik

Influence of deg. of turb. and turb. thread on deflection

p. 52
Fig. 17

NACA 65 - 612
l/l = 1,0
β_s = 150°

①	○	smooth vanes, no turb. screen
②	●	smooth vanes, turb. screen
③	▽	turb. thread on vanes

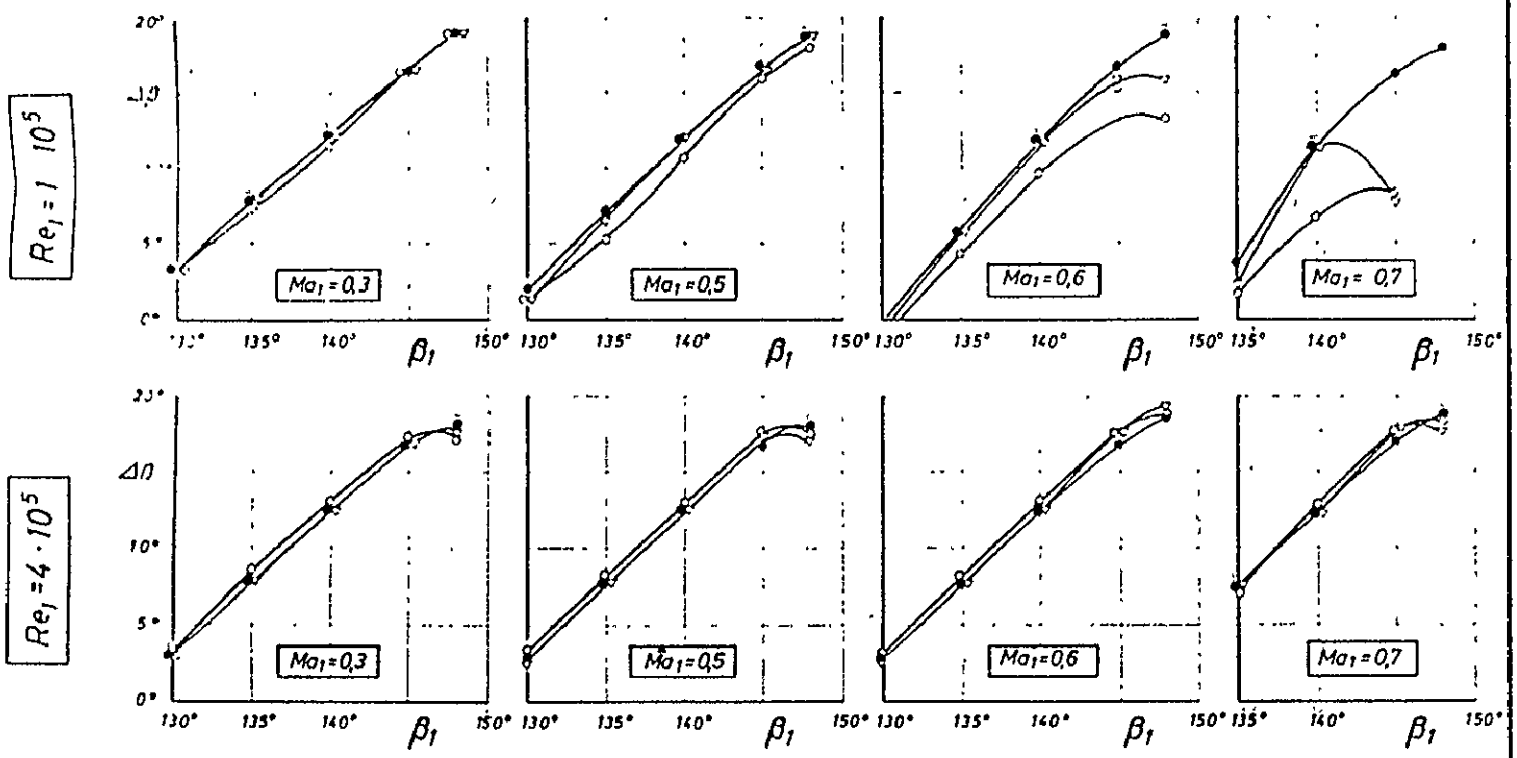

Bearbeitet Barsun Hahn | Datum 21.2.67 | Zeichnungsblatt Nr. | Bericht Nr. 68/34

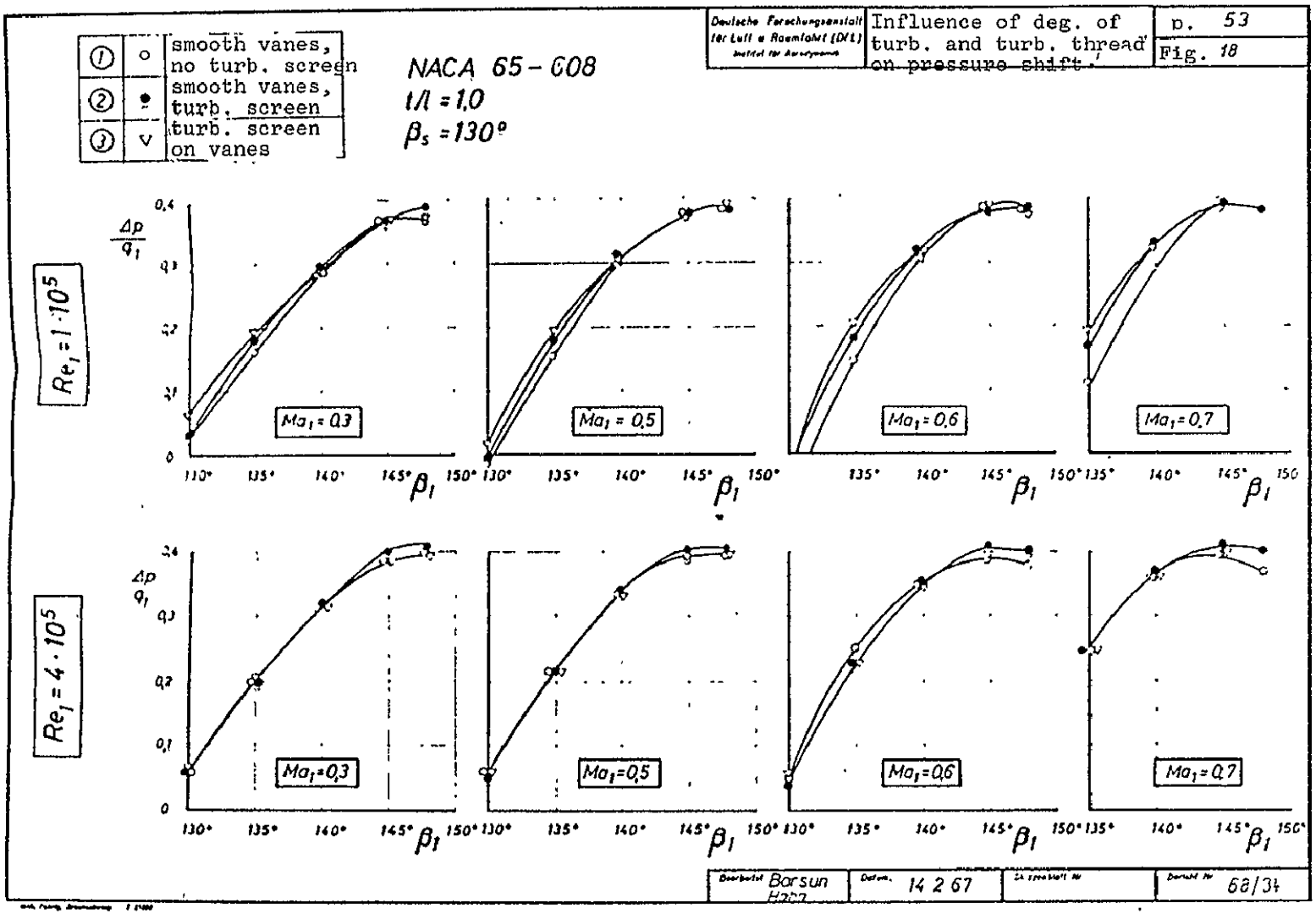
① ○ smooth vanes, no turb. screen
② ● smooth vanes, turb. screen
③ ▽ turb. screen on vanes
NACA 65 - 608
t/l = 1,0
β_s = 130°
Deutsche Forschungsanstalt für Luft u. Raumfahrt (DFL) Institut für Aerodynamik
Influence of deg. of turb. and turb. thread on pressure shift.
p. 53
Fig. 18
$Re_1 = 1 \cdot 10^5$
$Re_1 = 4 \cdot 10^5$
$\frac{\Delta p}{q_1}$
$Ma_1 = 0,3$
$Ma_1 = 0,5$
$Ma_1 = 0,6$
$Ma_1 = 0,7$
β_1
Bearbeitet Barsun Happ
Datum 14 2 67
Bericht Nr 68/34

ORIGINAL PAGE IS
OF POOR QUALITY

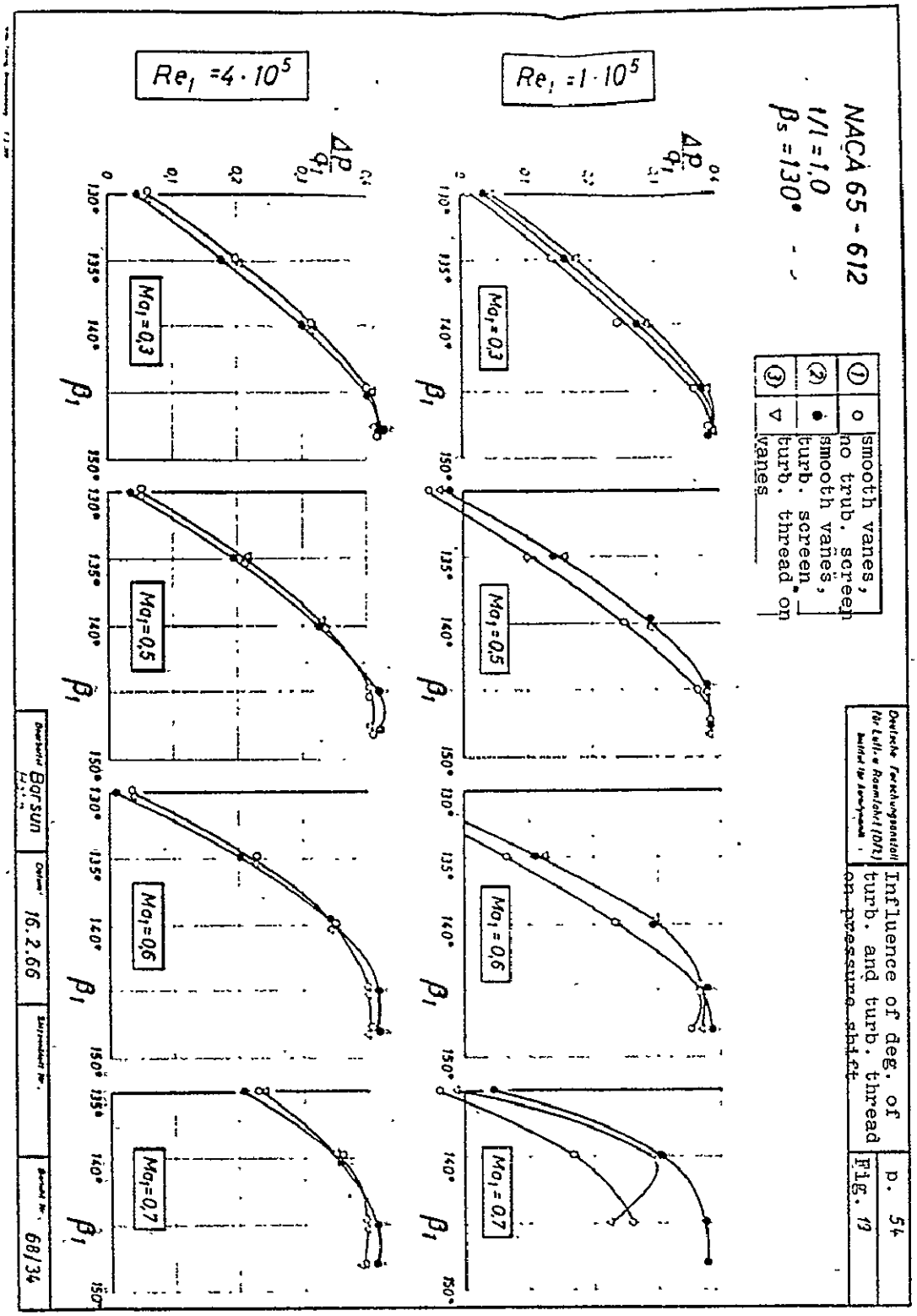

Deutsche Forschungsanstalt für Luft- u. Raumfahrt (DFL)

Influence of deg. of turb. and turb. thread on pressure distribution

Fig. 20

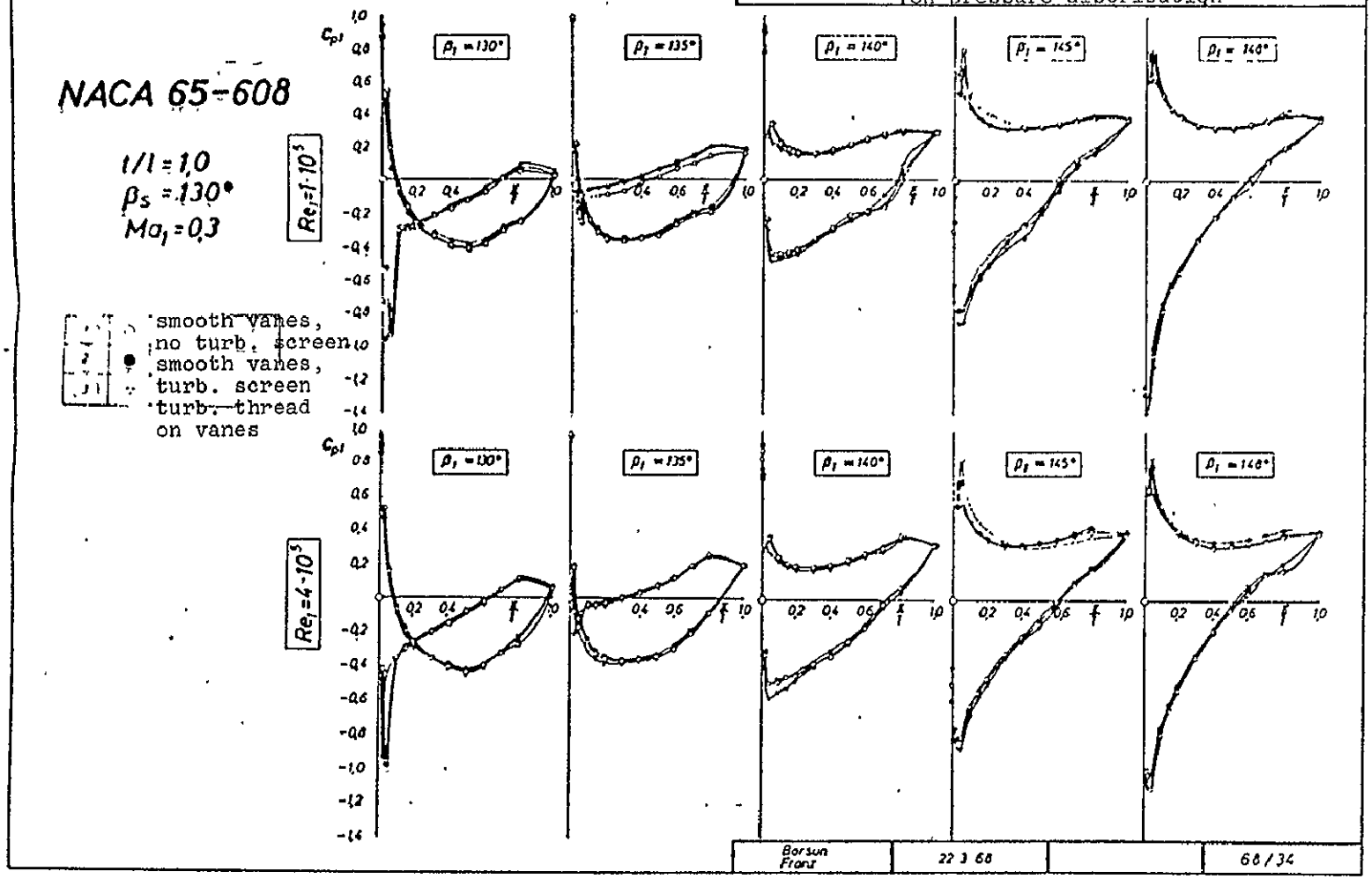

Borsun Franz	22 3 68		68/34

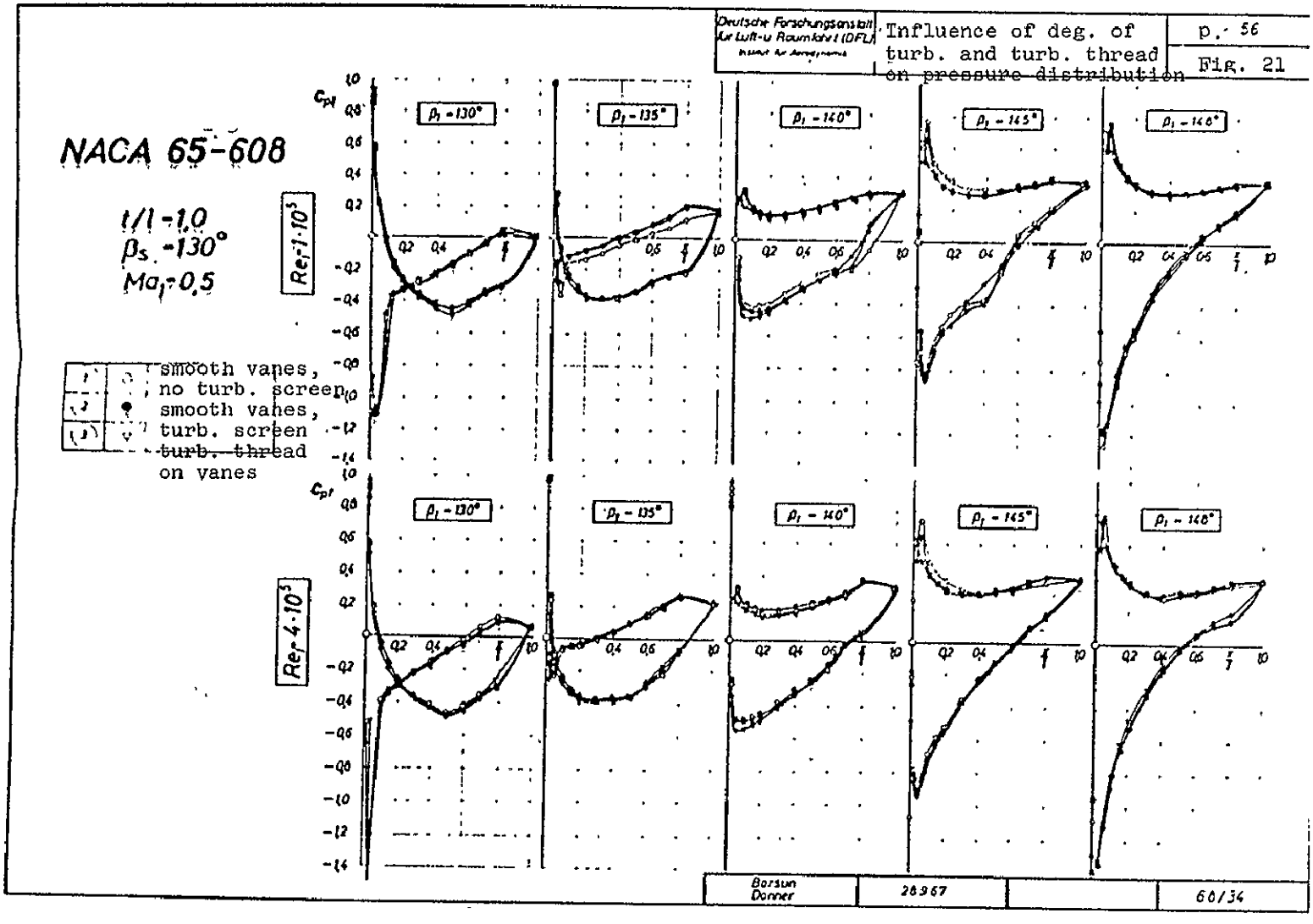

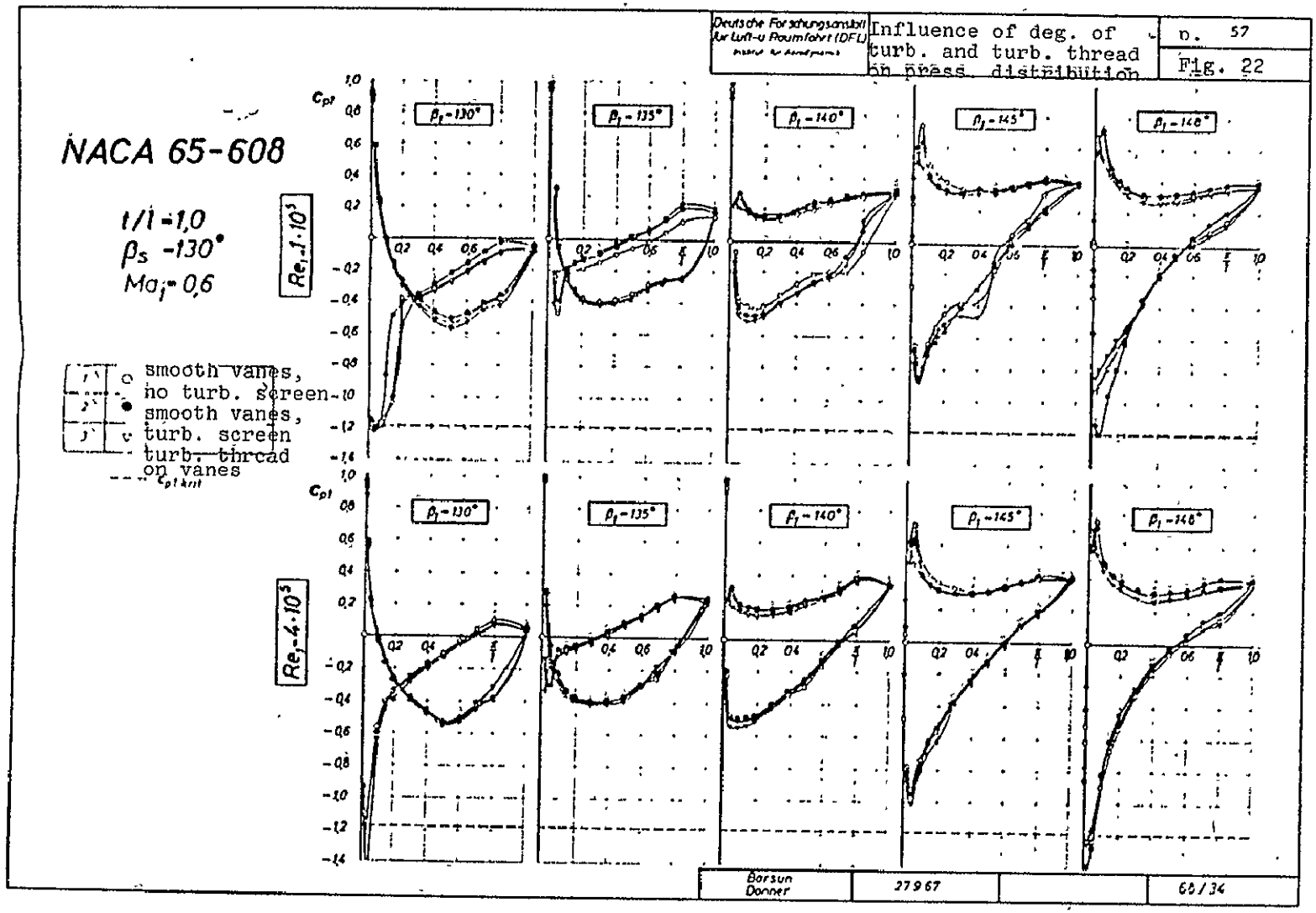
Deutsche Forschungsanstalt für Luft- u. Raumfahrt (DFL)
Influence of deg. of turb. and turb. thread on press. distribution
D. 57
Fig. 22
NACA 65-608
t/l = 1,0
β_s = -130°
Ma_1 = 0,6
$Re_1 \cdot 10^5$
$Re_1 \cdot 4 \cdot 10^5$
c_{p1}
β_1 = -130°
β_1 = -135°
β_1 = -140°
β_1 = -145°
β_1 = -148°
1 ○ smooth vanes, no turb. screen
2 ● smooth vanes, turb. screen
3 ▽ turb. thread on vanes
$c_{p1\,krit}$
Borsun
Donner
27967
60/34

ORIGINAL PAGE IS
OF POOR QUALITY

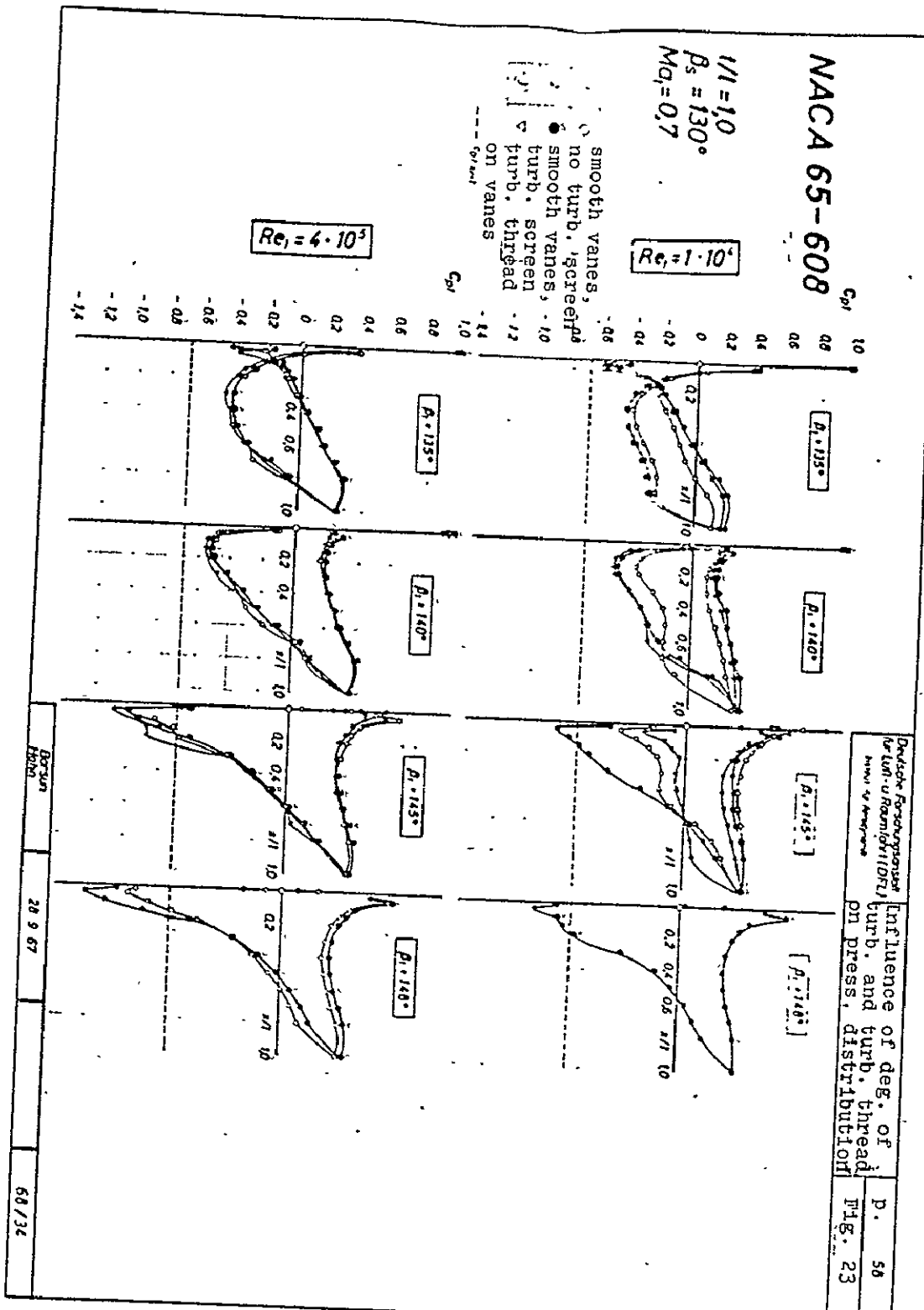

Deutsche Forschungsanstalt für Luft- u. Raumfahrt (DFL)
Institut für Aerodynamik

Influence of deg. of turb. and turb. thread on press. distribution

Fig. 24

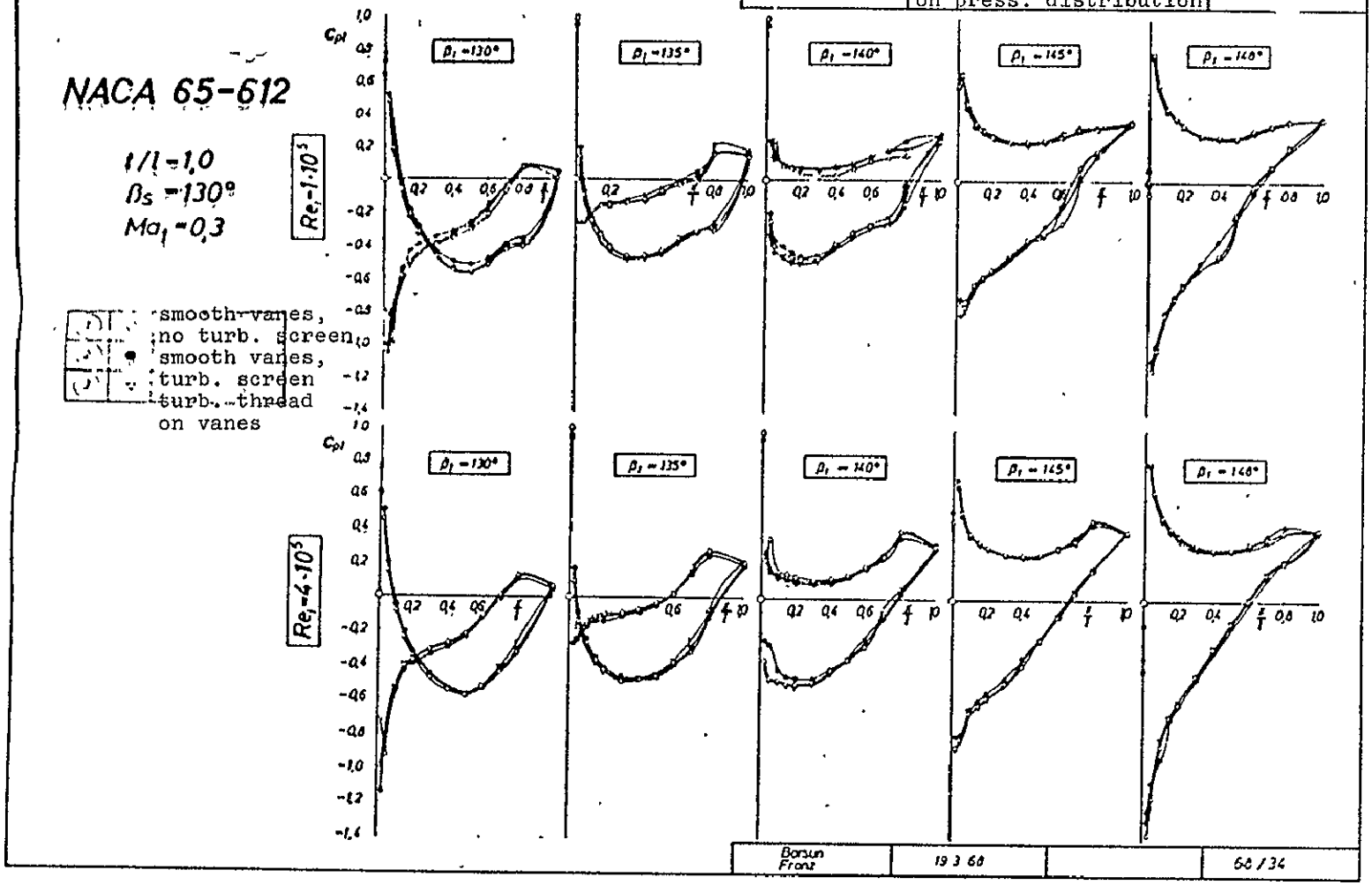

Borsun Frantz | 19 3 68 | | 68/34

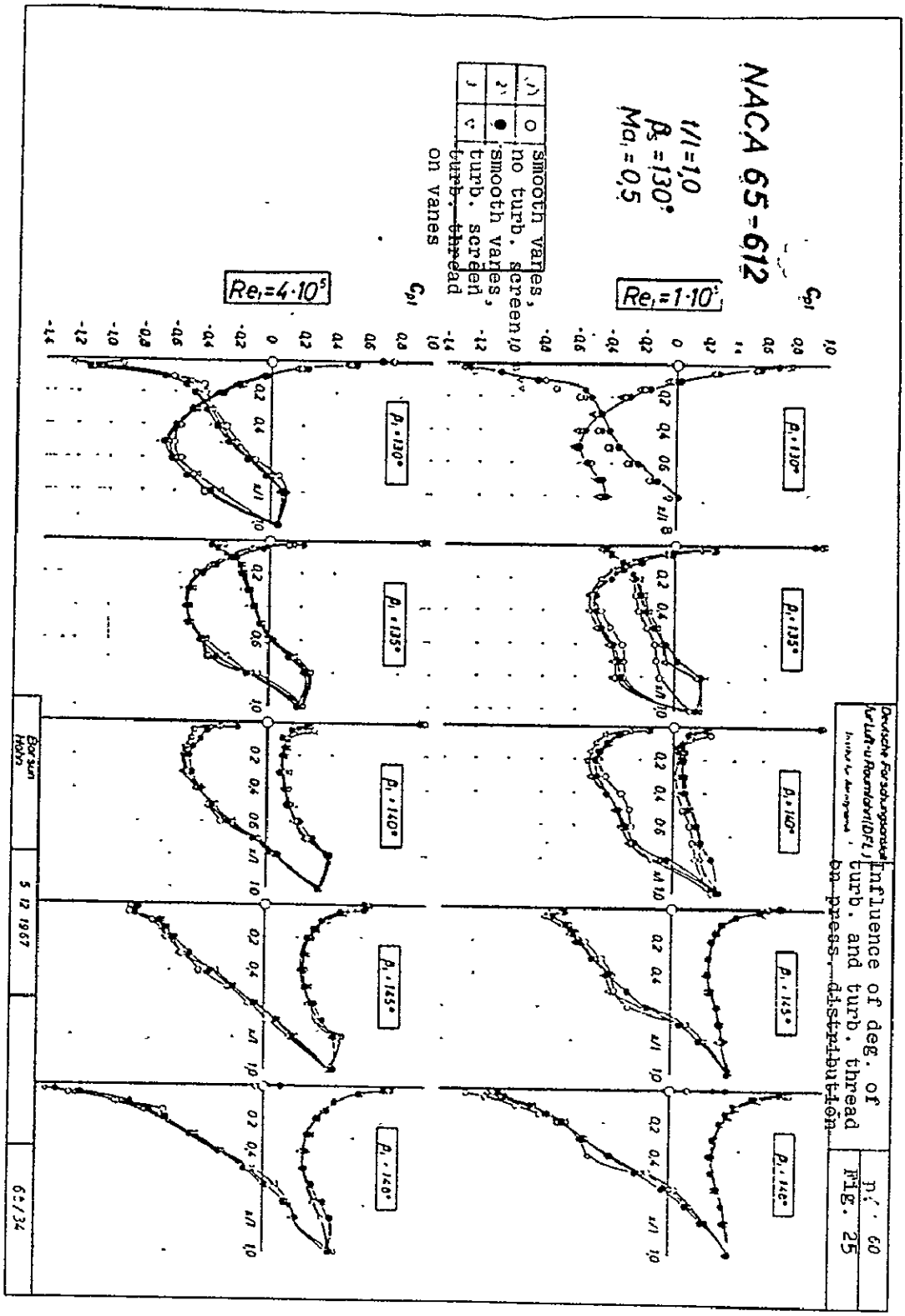

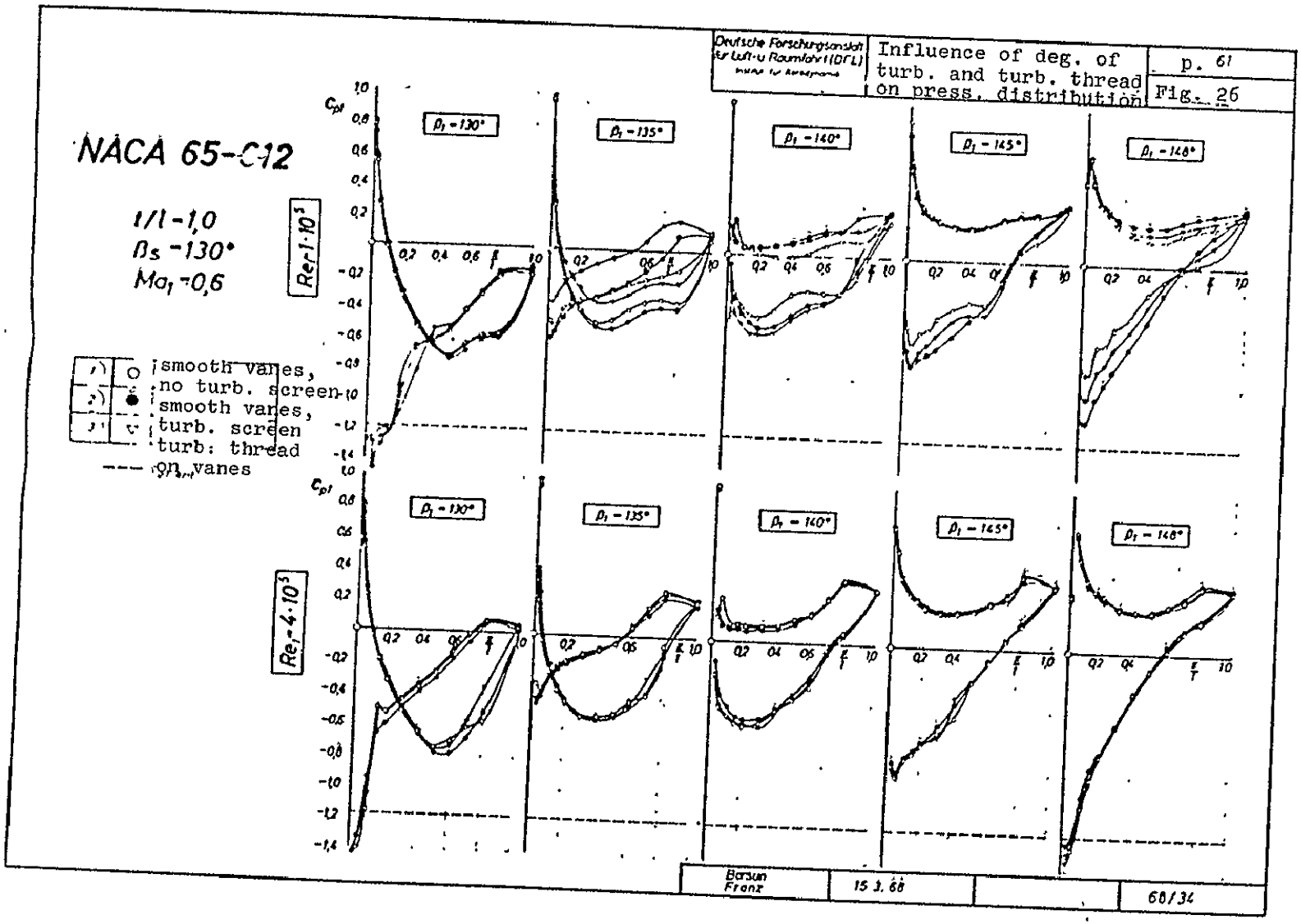
Deutsche Forschungsanstalt für Luft- u Raumfahrt (DFL)
Institut für Aerodynamik
Influence of deg. of turb. and turb. thread on press. distribution
p. 61
Fig. 26
NACA 65-012
1/l -1,0
β₅ -130°
Ma₁ -0,6
Re₁·10⁵
1) smooth vanes, no turb. screen
2) smooth vanes, turb. screen
3) turb: thread on vanes
β₁ = 130°
β₁ = 135°
β₁ = 140°
β₁ = 145°
β₁ = 148°
Re₁ = 4·10⁵
Borsun Franz
15 3. 68
68/34

Deutsche Forschungsanstalt für Luft u. Raumfahrt (DFL)
Institut für Aerodynamik

Influence of deg. of turb. and turb. thead on press. distribution

p. 62
Fig. 27

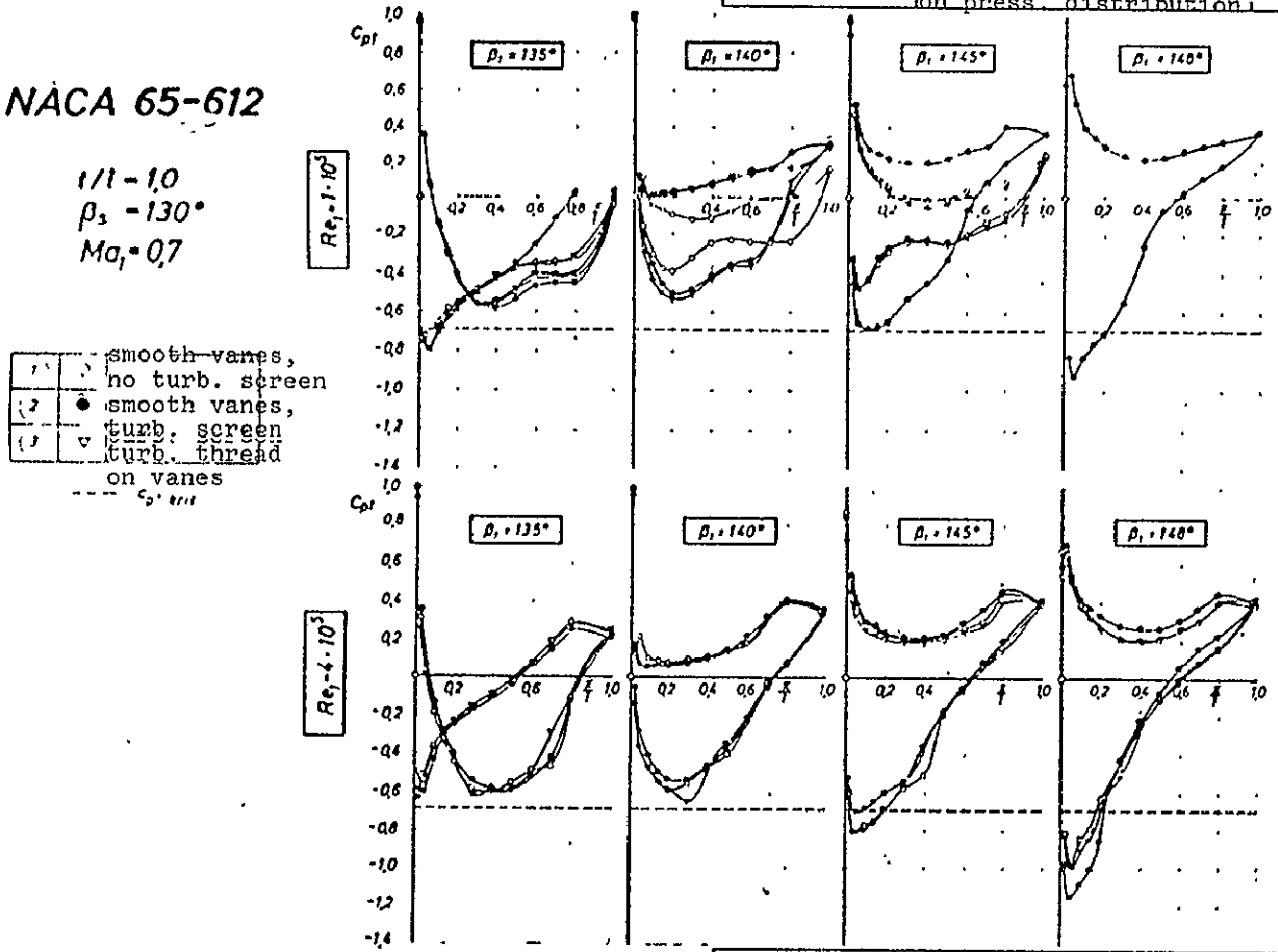

Borsun Donner	19 1 68		68/34

Deutsche Forschungsanstalt für Luft- und Raumfahrt (DFL) beim Max-Planck-Institut für Aerodynamik

Jet contraction coefficient as a function of deflection

p. 63

Fig. 28

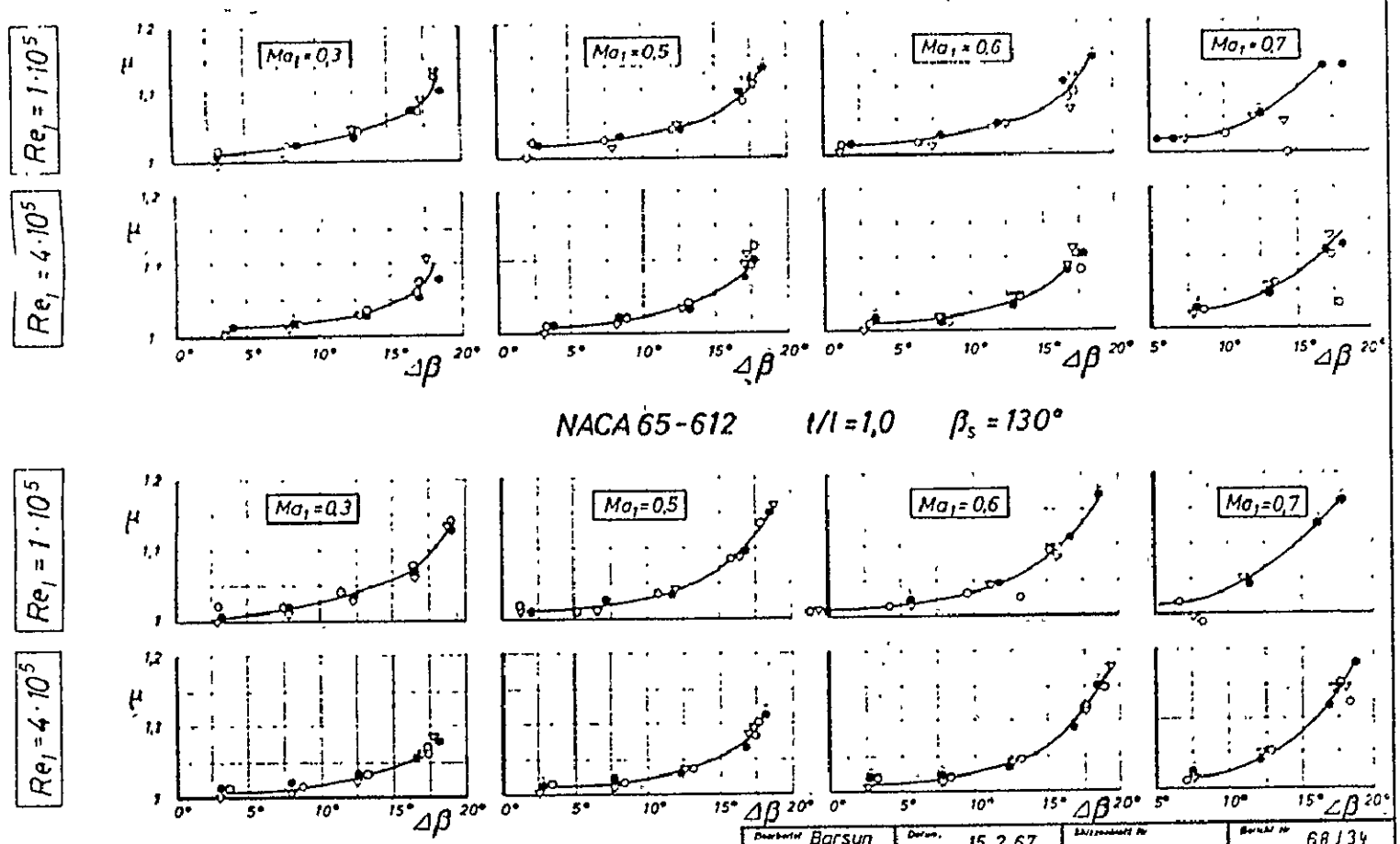

Bearbeitet	Datum		Bericht Nr
Barsun	15 2 67		68/34

Deutsche Forschungsanstalt für Luftfahrt (DFL) Institut für Aerodynamik	Profile coordinates and location of measurement points Profile NACA 65-608	p. 64 Table 1

Nose radius $100\frac{r_N}{l} = 0{,}425$

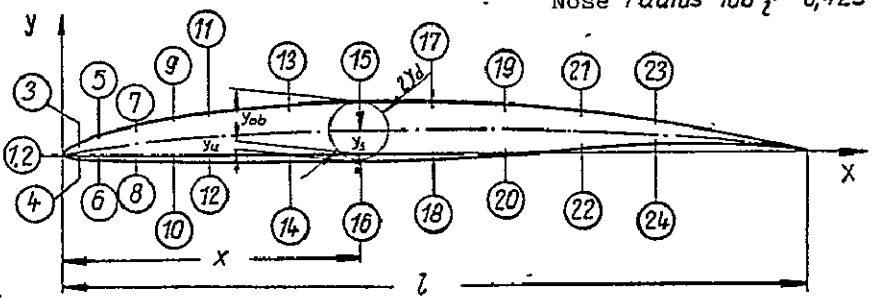

$100\frac{x}{l}$	$100\frac{y_s}{l}$	$100\frac{y_u}{l}$	$100\frac{y_{ob}}{l}$	$100\frac{y_d}{l}$	meas. pts. bottom	meas. pts. top
0	0	0	0	0	2	1
1,25	0,324	- 0,63	1,33	0,945	—	—
2,50	0,558	- 0,73	1,88	1,267	4	3
5,00	0,948	- 0,76	2,74	1,745	6	5
7,5	1,272	- 0,83	3,39	2,118	—	—
10	1,551	- 0,90	3,92	2,432	8	7
15	2,019	- 0,96	4,88	2,931	10	9
20	2,388	- 0,98	5,65	3,312	12	11
30	2,916	- 0,93	6,68	3,805	14	13
40	3,213	- 0,81	7,10	3,998	16	15
50	3,309	- 0,60	7,09	3,857	18	17
60	3,213	- 0,15	6,52	3,337	20	19
70	2,916	+ 0,35	5,45	2,553	22	21
80	2,388	+ 0,76	3,98	1,617	24	23
90	1,551	+ 0,90	2,24	0,664	—	—
95	0,948	+ 0,68	1,20	0,252	—	—
100	0	0	0	0	—	—

From report 65/5

Bearbeitet: Schuppe	Datum: 22.8.60	Skizzenblatt Nr.: -	Bericht Nr.: 68/34

Deutsche Forschungsanstalt für Luftfahrt (DFL)
Institut für Aerodynamik

Profile coordinates and location of measurement points

Profile NACA 65-612

Table 2

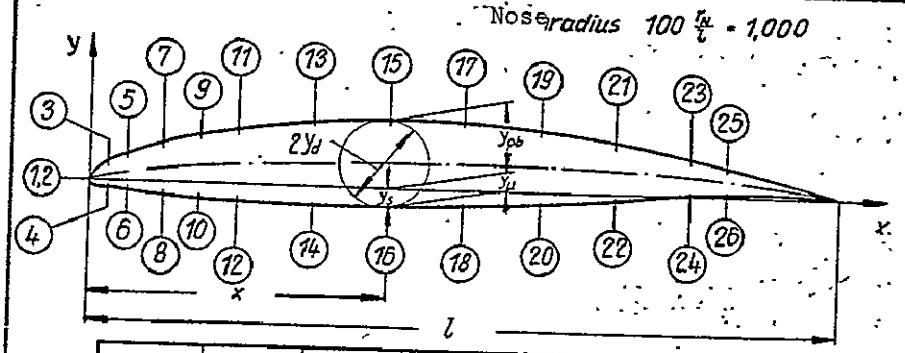

100 $\frac{x}{l}$	100 $\frac{y_s}{l}$	100 $\frac{y_z}{l}$	100 $\frac{y_{pb}}{l}$	100 $\frac{y_d}{l}$	meas. pts. bottom	meas. pts. top
0	0	0	0	0	2	1
1,25	0,324	-0,95	1,80	1,387	—	—
2,5	0,558	-1,29	2,61	1,912	4	3
5,0	0,948	-1,63	3,72	2,620	6	5
7,5	1,272	-1,83	4,51	3,178	—	—
10	1,551	-1,99	5,24	3,648	8	7
15	2,019	-2,31	6,44	4,394	10	9
20	2,388	-2,54	7,33	4,964	12	11
30	2,916	-2,84	8,52	5,704	14	13
40	3,213	-2,89	9,05	5,996	16	15
50	3,309	-2,57	8,96	5,800	18	17
60	3,213	-1,89	8,12	5,036	20	19
70	2,916	-0,98	6,76	3,870	22	21
80	2,388	0	4,91	2,466	24	23
90	1,551	+0,56	2,61	1,020	26	25
95	0,948	+0,51	1,33	0,390	—	—
100	0	0	0	0	—	—

at $100\frac{x}{l} = 85$

from Report 65/5

Bearbeitet	Datum	Skizzenblatt Nr.	Bericht Nr.
Schuppe	22.8.60		68/34

Re_1	β_1 [°]	ζ_{v1}	$\Delta p/q$	β_2 [°]	$\Delta\beta$ [°]	$c_{N\ Na.}$	$c_{N\ Dr.}$	μ	
$1 \cdot 10^5$	130	0,036	-0,008	128,3	1,7	0,053	0,060	1,011	NACA 65-608
	135	0,018	0,153	128,0	7,0	0,279	0,265	1,014	
	140	0,019	0,277	128,3	11,7	0,455	0,408	1,025	
	145	0,018	0,396	129,1	15,9	0,591	0,559	1,036	
	147,5	0,031	0,397	130,6	16,9	0,615	0,551	1,067	
$2 \cdot 10^5$	130	0,022	0,054	127,0	3,0	0,113	0,114	1,002	
	135	0,017	0,195	127,1	7,9	0,312	0,309	1,001	
	140	0,014	0,298	127,9	12,1	0,468	0,419	1,017	
	145	0,016	0,387	129,0	16,0	0,593	0,543	1,046	
	147,5	0,025	0,408	130,6	16,9	0,621	0,558	1,065	
$1 \cdot 10^5$	130	0,027	0,025	127,8	2,2	0,077	0,092	1,004	NACA 65-612
	135	0,026	0,145	128,3	6,7	0,267	0,263	1,011	
	140	0,028	0,265	129,1	10,9	0,425	0,374	1,016	
	145	0,020	0,359	129,4	15,6	0,581	0,503	1,061	
	147,5	0,019	0,407	129,7	17,8	0,644	0,534	1,084	
	150	0,027	0,397	130,9	19,1	0,676	0,596	1,148	
$2 \cdot 10^5$	130	0,019	0,020	128,8	1,2	0,042	0,098	0,998	
	135	0,017	0,196	127,7	7,3	0,291	0,275	0,992	
	140	0,016	0,297	128,1	11,9	0,461	0,428	1,014	
	145	0,013	0,385	128,6	16,4	0,606	0,532	1,059	
	147,5	0,016	0,420	129,0	18,5	0,662	0,568	1,086	
	150	0,058	0,398	131,5	18,5	0,656	0,598	1,125	

Grid arrangement $t/l = 1$

$\beta_S = 130°$

Vanes: smooth

Type of turb. (1) $Tu_1 \approx 0{,}3$ %

Boundary layer sucked off through top and bottom slots

Deutsche Forschungsanstalt für Luft- u. Raumfahrt (DFL) Institut für Aerodynamik

Results of wake measurements for Profile NACA 65-608

Table 6

NACA 65-608

$Re_1 = 1 \cdot 10^5$

		smooth vanes Tu ~ 0,2 – 1 %				smooth vanes with turb. scr. Tu ~ 2,5 – 4 %				vanes with turb. thread Tu ~ 0,2 – 1 %			
β_1 [°]	Ma_1	ζ_{v1}	$\Delta p/q_1$	$\Delta\vartheta$ [°]	μ	ζ_{v1}	$\Delta p/q_1$	$\Delta\vartheta$ [°]	μ	ζ_{v1}	$\Delta p/q_1$	$\Delta\vartheta$ [°]	μ
130	0,3	0,030	0,021	3,1	1,011	0,031	0,029	3,1	1,011	0,035	0,063	3,2	0,994
	0,4	0,039	0,010	2,9	1,015	0,039	0,014	3,1	1,016	0,043	0,043	2,8	0,990
	0,5	0,046	-0,02	2,6	1,020	0,043	0	2,8	1,018	0,047	0,017	2,1	0,995
	0,6	0,060	-0,07	1,3	1,015	0,054	-0,04	1,9	1,014	0,066	-0,06	1,2	1,004
	0,65	0,072	-0,18	-0,6	1,010	0,065	-0,09	1,2	1,013	0,081	-0,18	-1,8	0,987
135	0,3	0,026	0,162	8,0	1,023	0,021	0,181	8,6	1,023	0,023	0,192	7,9	1,000
	0,4	0,032	0,158	7,6	1,021	0,025	0,175	8,6	1,029	0,024	0,188	8,0	1,014
	0,5	0,036	0,155	7,5	1,024	0,027	0,181	8,5	1,030	0,027	0,194	7,9	1,014
	0,6	0,041	0,147	6,5	1,018	0,037	0,182	8,1	1,026	0,031	0,204	7,6	1,012
	0,65	0,043	0,124	6,0	1,024								
	0,7	0,054	0,109	5,5	1,021	0,045	0,169	6,8	1,020	0,040	0,193	7,4	1,020
	0,75	0,057	0,077	4,8	1,025	0,053	0,148	5,8	1,016	0,056	0,133	5,7	1,016
	0,78									0,074	0,052	3,7	1,007
	0,8												
	0,83												
140	0,3	0,027	0,285	12,9	1,039	0,019	0,296	12,8	1,035	0,018	0,283	12,6	1,043
	0,4	0,029	0,297	12,6	1,032	0,023	0,298	12,7	1,038	0,023	0,295	12,5	1,037
	0,5	0,030	0,301	12,5	1,039	0,021	0,310	12,6	1,041	0,020	0,304	12,5	1,045
	0,6	0,037	0,306	12,3	1,042	0,027	0,317	12,5	1,046	0,025	0,317	12,4	1,040
	0,7	0,055	0,289	10,3	1,028	0,028	0,331	12,6	1,057	0,030	0,323	12,2	1,054
	0,75									0,035	0,323	12,0	1,050
	0,8	0,078	0,248	8,2	1,019	0,035	0,337	12,5	1,068	0,056	0,298	10,4	1,045
	0,85	0,081	0,240	8,8	1,037	0,050	0,320	11,7	1,064	0,072	0,261	10,0	1,050
	0,9					0,094	0,260	9,0	1,036				
145	0,3	0,042	0,368	17,0	1,069	0,034	0,369	16,8	1,072	0,020	0,371	17,2	1,088
	0,4	0,044	0,375	17,0	1,071	0,037	0,373	16,9	1,079	0,023	0,385	17,4	1,084
	0,5	0,046	0,377	17,0	1,082	0,030	0,378	16,9	1,096	0,021	0,373	17,3	1,113
	0,6	0,053	0,384	17,1	1,090	0,034	0,379	16,8	1,108	0,024	0,389	17,2	1,115
	0,65	0,063	0,381	17,0	1,093					0,027	0,389	17,2	1,123
	0,7	0,137	0,389	14,6	0,998	0,036	0,382	17,0	1,130	0,070	0,391	14,2	1,046
	0,75									0,106	0,383	12,9	1,010
	0,8					0,071	0,371	15,5	1,108				
	0,85					0,096	0,367	14,6	1,088				
148	0,3	0,046	0,368	18,3	1,126	0,055	0,389	18,6	1,102	0,039	0,372	18,3	1,128
	0,4	0,048	0,379	18,0	1,119	0,053	0,382	18,6	1,122	0,040	0,383	18,0	1,124
	0,5	0,053	0,386	17,6	1,118	0,055	0,384	18,5	1,139	0,057	0,392	17,6	1,107
	0,55	0,067	0,380	17,4	1,115					0,080	0,381	17,6	1,104
	0,6	0,097	0,380	16,9	1,086	0,062	0,385	18,6	1,145	0,124	0,375	17,1	1,066
	0,65	0,182	0,360	16,2	1,012	0,068	0,380	18,8	1,158				
	0,7					0,097	0,382	18,3	1,131				
	0,75												

$Re_2 = 4 \cdot 10^5$

	smooth vanes Tu ~ 0,2 – 1 %				smooth vanes with turb. scr. Tu ~ 2,5 – 4 %				smooth vanes with turb. thread Tu ~ 0,2 – 1 %			
ζ_{v1}	$\Delta p/q_1$	$\Delta\vartheta$ [°]	μ	ζ_{v1}	$\Delta p/q_1$	$\Delta\vartheta$ [°]	μ	ζ_{v1}	$\Delta p/q_1$	$\Delta\vartheta$ [°]	μ
0,016	0,061	3,7	1,013	0,022	0,054	3,8	1,012	0,029	0,066	3,5	1,004
0,018	0,066	3,7	1,011	0,025	0,056	3,5	1,014	0,025	0,064	3,1	1,000
0,022	0,062	3,5	1,010	0,027	0,051	3,5	1,012	0,028	0,061	3,2	1,003
0,030	0,048	3,2	1,010	0,033	0,036	3,3	1,015	0,036	0,053	2,8	1,000
0,043	0,025	3,0	1,010	0,051	0,015	3,0	1,009	0,045	0,031	2,8	1,005
0,013	0,198	8,6	1,019	0,012	0,197	8,5	1,018	0,013	0,203	8,1	1,009
0,012	0,208	8,5	1,017	0,012	0,206	8,5	1,018				
0,013	0,214	8,6	1,022	0,014	0,216	8,5	1,019	0,015	0,215	8,3	1,017
0,015	0,249	8,5	1,017	0,014	0,228	8,4	1,021	0,015	0,226	8,0	1,017
0,018	0,244	8,4	1,025	0,017	0,243	8,3	1,025	0,017	0,244	8,0	1,020
0,032	0,251	8,1	1,025	0,024	0,249	8,1	1,031	0,025	0,265	8,1	1,023
0,083	0,107	4,5	1,001					0,087	0,094	3,5	0,988
0,012	0,315	13,4	1,036	0,014	0,320	13,2	1,027	0,013	0,316	13,1	1,030
0,012	0,324	13,1	1,034	0,013	0,330	13,0	1,027				
0,012	0,331	13,1	1,040	0,015	0,340	13,2	1,034	0,014	0,334	13,1	1,037
0,012	0,348	13,1	1,046	0,024	0,353	13,1	1,032	0,014	0,345	13,1	1,046
0,014	0,359	13,4	1,062	0,023	0,368	13,2	1,045	0,015	0,358	13,2	1,058
0,016	0,363	13,5	1,084	0,025	0,372	13,2	1,066	0,017	0,370	13,3	1,076
0,026	0,361	13,5	1,090	0,034	0,376	12,7	1,065	0,025	0,365	13,2	1,085
0,079	0,316	10,1	1,036	0,066	0,352	11,3	1,045	0,072	0,319	10,0	1,040
0,035	0,384	16,9	1,059	0,028	0,399	17,0	1,053	0,019	0,385	16,9	1,073
0,032	0,386	16,9	1,071	0,027	0,399	17,1	1,067	0,018	0,387	17,1	1,086
0,030	0,387	17,5	1,096	0,029	0,402	17,0	1,077	0,019	0,392	17,1	1,096
0,036	0,391	17,5	1,106	0,036	0,408	16,8	1,082	0,020	0,395	17,1	1,112
								0,021	0,398	17,2	1,121
0,057	0,393	17,3	1,106	0,038	0,410	17,1	1,106	0,022	0,397	17,3	1,135
0,099	0,394	17,1	1,072					0,024	0,398	17,8	1,156
				0,059	0,402	17,0	1,121	0,071	0,383	15,8	1,103
				0,110	0,379	14,2	1,059				
0,050	0,397	17,1	1,075	0,054	0,409	18,3	1,076	0,031	0,393	17,5	1,104
0,048	0,393	17,0	1,091	0,067	0,403	17,9	1,077	0,034	0,392	17,5	1,113
0,044	0,393	17,7	1,121	0,060	0,404	17,8	1,098	0,044	0,395	17,2	1,111
0,114	0,381	17,3	1,064					0,060	0,395	16,9	1,099
0,115	0,378	17,7	1,082	0,075	0,400	17,8	1,105	0,084	0,391	16,8	1,088
0,133	0,375	17,8	1,078					0,093	0,389	17,2	1,097
0,192	0,367	17,9	1,033	0,093	0,400	18,1	1,116				
				0,128	0,395	17,9	1,097				

Bearbeiter:	Datum:	Skizzenblatt Nr.:	Bericht Nr.:
Da/Sch	28.2.1967		68/34

ORIGINAL PAGE IS
OF POOR QUALITY

Deutsche Forschungsanstalt für Luft- u. Raumfahrt (DFL) Institut für Aerodynamik

Results of wake measurements for NACA 65-612 Profile

p. 68

Table 7

NACA 65 - 612

$Re_1 = 1 \cdot 10^5$

β_1 [°]	y/a_1	smooth vanes Tu ≈ 0,2 – 1 % ζ_{y1}	$\Delta p/q_1$	$\Delta\vartheta$ [°]	μ	smooth vanes, with turb. scr. Tu ≈ 2,5 – 4 % ζ_{y1}	$\Delta p/q_1$	$\Delta\vartheta$ [°]	μ	vanes with turb. thread Tu ≈ 0,2 – 1 % ζ_{y1}	$\Delta p/q_1$	$\Delta\vartheta$ [°]	μ
130	0,3	0,033	0,010	2,9	1,019	0,040	0,035	3,1	1,004	0,035	0,046	3,0	1,001
	0,4	0,013	-0,02	2,0	1,013	0,044	0,011	2,8	1,011	0,039	0,021	2,7	1,008
	0,5	0,047	-0,06	1,3	1,017	0,052	-0,02	2,0	1,011	0,048	-0,04	1,3	1,009
	0,55	0,053	-0,10	0,6	1,018	0,058	-0,07	1,4	1,018				
	0,6	0,075	-0,18	-1,0	1,008	0,073	-0,14	-0,1	1,010	0,066	-0,16	-0,8	1,008
	0,63	0,115	-0,48	-4,9	0,991					0,092	-0,24	-1,9	0,999
	0,65												
135	0,3	0,033	0,143	7,4	1,021	0,029	0,161	7,8	1,019	0,027	0,181	7,8	1,010
	0,4	0,043	0,125	6,4	1,016	0,035	0,149	7,7	1,025	0,032	0,168	7,0	1,007
	0,5	0,051	0,099	5,3	1,012	0,038	0,140	7,1	1,025	0,035	0,158	6,6	1,011
	0,55					0,041	0,140	7,1	1,027				
	0,6	0,058	0,066	4,3	1,012	0,051	0,110	5,8	1,020	0,051	0,125	5,8	1,013
	0,65					0,060	0,072	4,6	1,017				
	0,7	0,066	-0,04	1,7	1,007	0,065	0,040	3,6	1,012	0,075	-0,01	2,3	1,005
	0,75	0,077	-0,06	2,3	1,015								
	0,78												
	0,8												
140	0,3	0,038	0,245	11,5	1,039	0,029	0,275	12,3	1,036	0,023	0,289	12,2	1,029
	0,4	0,040	0,266	11,4	1,029	0,029	0,286	12,2	1,035	0,024	0,290	12,1	1,035
	0,5	0,046	0,250	10,7	1,034	0,034	0,290	11,9	1,035	0,027	0,292	12,0	1,041
	0,6	0,059	0,234	9,6	1,031	0,038	0,293	11,8	1,042	0,031	0,298	11,6	1,042
	0,7	0,084	0,167	6,7	1,015	0,042	0,306	11,4	1,043	0,041	0,289	11,2	1,051
	0,75									0,058	0,245	10,1	1,056
	0,8	0,093	0,153	6,7	1,027	0,052	0,290	10,5	1,053				
	0,85												
	0,88												
	0,9												
145	0,3	0,027	0,363	16,5	1,078	0,028	0,374	16,5	1,068	0,025	0,382	16,5	1,064
	0,4	0,032	0,361	16,0	1,078	0,029	0,371	16,7	1,084	0,026	0,378	16,4	1,076
	0,5	0,035	0,365	15,9	1,085	0,028	0,377	16,8	1,096	0,030	0,380	16,5	1,087
	0,6	0,040	0,364	15,4	1,093	0,031	0,376	16,7	1,111	0,039	0,366	15,7	1,096
	0,65	0,045	0,355	14,6	1,092					0,109	0,300	10,9	1,013
	0,7	0,128	0,259	8,3	0,988	0,030	0,374	16,3	1,130	0,130	0,226	7,8	0,996
	0,75					0,058	0,362	15,0	1,105				
	0,8					0,111	0,323	12,5	1,055				
	0,85												
	0,9												
148	0,3	0,025	0,386	19,0	1,140	0,034	0,386	18,9	1,129	0,025	0,390	18,9	1,134
	0,4	0,028	0,384	18,7	1,145	0,035	0,392	18,6	1,131	0,027	0,391	19,0	1,145
	0,5	0,042	0,386	18,0	1,135	0,038	0,385	18,6	1,150	0,030	0,382	18,7	1,161
	0,55	0,063	0,387	17,0	1,107					0,031	0,386	18,5	1,164
	0,6	0,121	0,353	13,3	1,024	0,039	0,386	18,8	1,171	0,086	0,371	15,7	1,084
	0,65	0,159	0,306	10,3	0,979					0,121	0,296	12,2	1,058
	0,7					0,066	0,378	18,0	1,161				
	0,75					0,137	0,355	14,7	1,084				
	0,8					0,154	0,309	13,0	1,065				

$Re_2 = 4 \cdot 10^5$

β_1 [°]	y/a_1	smooth vanes Tu ≈ 0,2 – 1 % ζ_{y1}	$\Delta p/q_1$	$\Delta\vartheta$ [°]	μ	smooth vanes, with turb. scr. Tu ≈ 2,5 – 4 % ζ_{y1}	$\Delta p/q_1$	$\Delta\vartheta$ [°]	μ	vanes with turb. thread Tu ≈ 0,2 – 1 % ζ_{y1}	$\Delta p/q_1$	$\Delta\vartheta$ [°]	μ
130	0,3	0,017	0,060	3,4	1,009	0,022	0,044	3,1	1,010	0,020	0,062	3,0	1,000
	0,4	0,020	0,059	3,5	1,011	0,021	0,039	3,0	1,013	0,023	0,054	3,0	1,005
	0,5	0,023	0,049	3,4	1,014	0,029	0,035	2,9	1,010	0,024	0,048	2,6	1,003
	0,55					0,028	0,024	2,5	1,011				
	0,6	0,030	0,034	3,1	1,015	0,040	0,010	2,9	1,016	0,033	0,037	2,6	1,005
	0,63												
	0,65	0,078	-0,17	-1,1	0,996					0,097	-0,12	0	0,989
135	0,3	0,014	0,201	8,6	1,016	0,015	0,178	7,9	1,019	0,013	0,206	7,9	1,004
	0,4	0,013	0,205	8,4	1,017	0,017	0,186	7,9	1,018				
	0,5	0,014	0,213	8,2	1,017	0,016	0,194	7,8	1,020	0,015	0,216	7,8	1,009
	0,55												
	0,6	0,017	0,224	8,1	1,018	0,018	0,203	7,6	1,021	0,015	0,225	7,8	1,014
	0,65	0,019	0,226	7,7	1,016								
	0,7	0,023	0,229	7,3	1,013	0,034	0,207	7,5	1,019	0,018	0,238	7,6	1,017
	0,75	0,039	0,209	6,4	1,006	0,058	0,171	6,0	1,006	0,024	0,238	7,6	1,020
	0,78									0,054	0,199	6,1	1,002
	0,8												
140	0,3	0,013	0,315	13,1	1,031	0,017	0,301	12,6	1,030	0,013	0,314	12,5	1,023
	0,4	0,013	0,328	13,3	1,033								
	0,5	0,013	0,336	13,0	1,036	0,019	0,328	12,5	1,029	0,015	0,332	12,6	1,032
	0,6	0,014	0,347	13,1	1,045	0,019	0,343	12,4	1,033	0,015	0,342	12,5	1,039
	0,7	0,015	0,358	12,9	1,054	0,022	0,356	12,3	1,042	0,017	0,353	12,4	1,049
	0,75												
	0,8	0,024	0,359	12,4	1,064	0,032	0,361	11,9	1,048	0,021	0,361	12,5	1,066
	0,85	0,080	0,285	8,6	1,015	0,055	0,333	10,6	1,040	0,044	0,328	10,5	1,051
	0,88									0,097	0,223	6,8	1,010
	0,9					0,130	0,169	6,3	1,003				
145	0,3	0,016	0,400	17,3	1,068	0,021	0,401	16,8	1,055	0,015	0,407	17,0	1,059
	0,4	0,016	0,406	17,5	1,078					0,017	0,408	17,2	1,071
	0,5	0,015	0,403	17,6	1,098	0,023	0,418	16,8	1,066	0,016	0,405	17,4	1,093
	0,6	0,017	0,398	17,6	1,120	0,022	0,414	16,8	1,090	0,017	0,401	17,6	1,118
	0,65												
	0,7	0,019	0,394	17,7	1,147	0,024	0,413	17,0	1,117	0,020	0,397	17,9	1,147
	0,75	0,027	0,389	17,2	1,150	0,027	0,411	16,6	1,125	0,026	0,391	17,5	1,155
	0,8	0,104	0,370	14,3	1,056	0,056	0,397	15,5	1,103	0,100	0,376	13,5	1,044
	0,85					0,116	0,344	13,1	1,058				
	0,9					0,154	0,287	10,9	1,036				
148	0,3	0,043	0,419	17,2	1,063	0,035	0,424	18,0	1,078	0,038	0,413	17,8	1,084
	0,4	0,053	0,417	17,1	1,064	0,036	0,426	18,0	1,087	0,051	0,412	17,1	1,071
	0,5	0,058	0,411	17,4	1,086	0,039	0,417	18,1	1,110	0,059	0,406	17,1	1,064
	0,55	0,052	0,411	17,9	1,111								
	0,6	0,049	0,406	18,9	1,146	0,036	0,415	18,7	1,147	0,031	0,393	19,4	1,177
	0,65	0,053	0,403	19,0	1,157					0,024	0,396	20,3	1,215
	0,7	0,096	0,394	18,4	1,123	0,037	0,410	18,7	1,177	0,068	0,369	17,6	1,144
	0,75					0,091	0,396	17,4	1,123				
	0,8					0,134	0,371	16,2	1,092				

Gearbeitet: | Datum: | Skizzenblatt Nr.: | Bericht Nr.: 68/34